© 2022. Published by The Company of Biologists Ltd | Development (2022) 149, dev200028. doi:10.1242/dev.200028

STEM CELLS AND REGENERATION

RESEARCH ARTICLE

Olig2 defines a subset of neural stem cells that produce specific olfactory bulb interneuron subtypes in the subventricular zone of adult mice

Ángela del Águila[1,*], Mike Adam[1], Kristy Ullom[1], Nicholas Shaw[1,2], Shenyue Qin[1], Jacqueline Ehrman[1], Diana Nardini[3], Joseph Salomone[1], Brian Gebelein[1], Q. Richard Lu[3,4], Steven S. Potter[1,4], Ronald Waclaw[1,3,4], Kenneth Campbell[1,4,5] and Masato Nakafuku[1,4,6,‡]

ABSTRACT

Distinct neural stem cells (NSCs) reside in different regions of the subventricular zone (SVZ) and generate multiple olfactory bulb (OB) interneuron subtypes in the adult brain. However, the molecular mechanisms underlying such NSC heterogeneity remain largely unknown. Here, we show that the basic helix-loop-helix transcription factor Olig2 defines a subset of NSCs in the early postnatal and adult SVZ. Olig2-expressing NSCs exist broadly but are most enriched in the ventral SVZ along the dorsoventral axis complementary to dorsally enriched Gsx2-expressing NSCs. Comparisons of Olig2-expressing NSCs from early embryonic to adult stages using single cell transcriptomics reveal stepwise developmental changes in their cell cycle and metabolic properties. Genetic studies further show that cross-repression contributes to the mutually exclusive expression of Olig2 and Gsx2 in NSCs/progenitors during embryogenesis, but that their expression is regulated independently from each other in adult NSCs. Finally, lineage-tracing and conditional inactivation studies demonstrate that Olig2 plays an important role in the specification of OB interneuron subtypes. Altogether, our study demonstrates that Olig2 defines a unique subset of adult NSCs enriched in the ventral aspect of the adult SVZ.

KEY WORDS: Neural stem cell, Adult neurogenesis, Regional identity, Olfactory bulb, Development

INTRODUCTION

Neural stem cells (NSCs) persist and continuously produce new neurons in a few specialized regions of the adult mammalian brain, including the subventricular zone (SVZ) lining the lateral ventricle (LV) (Nakafuku and Grande, 2020). In these so-called 'neurogenic niches', NSCs remain mostly quiescent or divide infrequently (Götz et al., 2016). These quiescent stem cells (qNSCs) share some features with radial glia in embryos and astrocytes in adults, such as the expression of the intermediate filament protein Nestin and glial high-affinity glutamate transporter GLAST (Pastrana et al., 2009). However, a subset of these qNSCs are mobilized to become activated NSCs (aNSCs) and generate rapidly proliferating secondary progenitors called transient amplifying progenitors (TAPs). These TAPs subsequently differentiate into neuroblasts (NBs) and/or glial cells and migrate to their destinations, such as the olfactory bulb (OB), where they integrate into the existing circuitry.

Recent studies have identified many common regulatory mechanisms between these adult NSCs/progenitors and their embryonic counterparts (Götz et al., 2016; Nakafuku and del Águila, 2020). For example, the homeodomain transcription factor (TF) Gsx2 is expressed in a subset of NSCs/progenitors in both the developing ventral telencephalon and the adult SVZ, and plays an important role in the generation of specific neuronal subtypes in the OB (Toresson et al., 2000; Toresson and Campbell, 2001; Yun et al., 2001, 2003; Waclaw et al., 2009; Wang et al., 2013; Qin et al., 2017; López-Juárez et al., 2013). Likewise, the basic helix-loop-helix (bHLH) TF Ascl1 is commonly expressed and plays an essential role in neurogenesis in NSCs/progenitors in the embryonic ventral telencephalon and adult SVZ (Torii et al., 1999; Casarosa et al., 1999; Yun et al., 2002; Wang et al., 2009; Andersen et al., 2014).

Another important common feature between embryos and adults is that NSCs/progenitors in different regions are heterogeneous and produce distinct subtypes of neurons (Götz et al., 2016). For example, NSCs/progenitors in different parts of the ventral telencephalon generate distinct subtypes of OB interneurons during embryogenesis (Stenman et al., 2003; Kohwi et al., 2007; Long et al., 2007; Waclaw et al., 2009; Qin et al., 2017). NSCs that reside in distinct subregions of the adult SVZ also produce different OB interneuron subtypes (Young et al., 2007; Merkle et al., 2007, 2014; López-Juárez et al., 2013; Fuentealba et al., 2015; Delgado and Lim, 2015; Lledo and Valley, 2016; Paul et al., 2017). However, the molecular mechanisms underlying such heterogeneity of adult NSCs remain largely unknown.

It is widely known that the bHLH TF Olig2 is expressed in cells in the oligodendrocyte (OL) lineage and plays an essential role in their development (Emery and Lu, 2015). Importantly, Olig2 is also expressed in other neural cell types, including NSCs/progenitors (Takebayashi et al., 2002; Cai et al., 2007; Qin et al., 2017; Chapman et al., 2018). In this study, we show that Olig2 is expressed in a ventrally enriched subset of NSCs in the early postnatal and adult SVZ and plays an important role in the specification of OB interneuron subtypes. Single cell

[1]Division of Developmental Biology, Cincinnati Children's Hospital Research Foundation, 3333 Burnet Avenue, Cincinnati, OH 45229-3039, USA. [2]Department of Medical Science, University of Cincinnati College of Medicine, 3125 Eden Avenue, Cincinnati, OH 45267-0521, USA. [3]Division of Experimental Hematology and Cancer Biology, Cincinnati Children's Hospital Research Foundation, 3333 Burnet Avenue, Cincinnati, OH 45229-3039, USA. [4]Department of Pediatrics, University of Cincinnati College of Medicine, 3125 Eden Avenue, Cincinnati, OH 45267-0521, USA. [5]Division of Neurosurgery, Cincinnati Children's Hospital Research Foundation, 3333 Burnet Avenue, Cincinnati, OH 45229-3039, USA. [6]Department of Neurosurgery, University of Cincinnati College of Medicine, 3125 Eden Avenue, Cincinnati, OH 45267-0521, USA.
*Present address: Department of Anesthesiology, Duke University Medical Center, 134 Research Dr, Durham, NC 27710, USA.

‡Author for correspondence (masato.nakafuku@cchmc.org)

M.N., 0000-0001-7783-9005

Handling Editor: James Briscoe
Received 21 July 2021; Accepted 24 January 2022

Development (2022) 149, dev200028. doi:10.1242/dev.200028

transcriptomics and genetic studies also reveal important similarities and differences between Olig2-expressing NSCs/progenitors in the embryonic and postnatal brains.

RESULTS

Olig2 is expressed in a ventrally enriched subset of postnatal NSCs

In a search for molecular markers for NSCs, we found that the bHLH TF Olig2 is expressed in the adult SVZ (Fig. 1A-E). Similar to its embryonic expression (Takebayashi et al., 2002; Chapman et al., 2013, 2018), Olig2 expression was found broadly along the dorsoventral (DV) and mediolateral (ML) axes of the LV. However, the density of Olig2$^+$ cells among total cells in the dorsolateral (dl) SVZ is significantly lower than in other subdomains (Fig. 1F). Moreover, because both the density and total number of cells are much higher in the ventral (v) SVZ than in the lateral (l) and medial (m) SVZ subdomains (for details, see López-Juárez et al., 2013), the actual number of Olig2$^+$ cells is highest in the vSVZ among the four subdomains examined (Fig. 1F; the locations of distinct SVZ subdomains are indicated in the lower panel of Fig. 1C). By contrast, Gsx2$^+$ cells were predominantly detected in the dlSVZ. Moreover, although Olig2$^+$ and Gsx2$^+$ cells were found in all subdomains, few, if any, cells co-expressing both TFs were found (0 out of 63 Olig2$^+$ cells in the vSVZ and 0 out of 42 Gsx2$^+$ cells in the dlSVZ examined) (Fig. 1B-E,G). A similar regionally biased distribution of Olig2$^+$ and Gsx2$^+$ cells was also observed in the early postnatal day (P) 16 brain (Fig. 1F). Olig2$^+$ cells were also detected in the dorsal roof (callosal) region of the SVZ. However, this SVZ subdomain is immediately adjacent to the overlaying corpus callosum, where Olig2$^+$ oligodendrocytes are abundant. Therefore, it is difficult to distinguish Olig2$^+$ NSCs from Olig2$^+$ oligodendrocytes in this region. Along the anteroposterior (AP) axis of the LV, both Olig2$^+$ and Gsx2$^+$ cells were broadly detected (Fig. 1A-E), although few Olig2$^+$ cells were detected in the rostral migratory stream (RMS) or the most anterior or posterior portions of the SVZ, whereas a significant number of Gsx2$^+$ cells occurred in these regions (López-Juárez et al., 2013).

We next examined the cell types that express Olig2 in the NSC lineage. Although only a few Olig2$^+$ cells were immunopositive for glial fibrillary acidic protein (Gfap) or Dcx, a large fraction of Olig2$^+$ cells co-expressed the TFs Ascl1 and Dlx2, as well as the proliferation marker Ki67, in the vSVZ of the P16 and adult brain (Fig. 1H-N). Ascl1 is expressed in aNSCs and TAPs and plays an essential role in both the proliferation and neuronal differentiation of NSCs, whereas Dlx2 is mostly expressed in late-stage TAPs and NBs and promotes neurogenesis (Doetsch et al., 2002; Kohwi et al., 2007; Brill et al., 2008; López-Juárez et al., 2013; Andersen et al., 2014) (Fig. 1N). These results collectively support the idea that Olig2 is expressed in aNSCs and TAPs in the vSVZ (Fig. 1N), which is reminiscent of the expression pattern of Gsx2 in the dlSVZ (López-Juárez et al., 2013). Although we detected only a few Olig2$^+$/Gfap$^+$ cells, this might be because of a technical issue given that weak and/or diffuse cytoplasmic signals of Gfap staining in the postnatal SVZ often make it difficult to distinguish individual immunoreactive cells in conventional histology, unlike clear nuclear signals detectable by Ascl1 staining (Pastrana et al., 2009; López-Juárez et al., 2013). Moreover, more than 50% of Ascl1$^+$ cells in the vSVZ co-expressed Olig2 [55% (72 Ascl1$^+$/Olig2$^+$ cells among 130 Ascl1$^+$ cells examined) and 62% (120 Ascl1$^+$/Olig2$^+$ cells among 195 Ascl1$^+$ cells examined) in the adult and P16 brains, respectively], demonstrating that Olig2$^+$ cells are a predominant population among aNSCs/TAPs in the vSVZ.

Molecular characterization of Olig2-expressing NSCs by single cell transcriptomics

The aforementioned results demonstrate that Olig2 is expressed in the NSC lineage. However, it is still possible that some of these Olig2$^+$ cells are OLs newly generated from NSCs. In fact, it has been shown that a small, but significant, number of new OLs are generated by adult NSCs (Hack et al., 2005; Menn et al., 2006; Ortega et al., 2013). Recently, single cell RNA-sequencing (scRNA-seq) analysis has begun to be widely used to reveal molecular properties of postnatal NSCs and their progeny (Dulken et al., 2017; Yuzwa et al., 2017; Zywitza et al., 2018; Mizrak et al., 2019; Xie et al., 2020; Coré et al., 2020; Cebrian-Silla et al., 2021). To distinguish the expression of Olig2 in NSCs and other cell types, we also performed scRNA-seq analysis of the early postnatal and adult SVZ. A thin strip of tissue around the LV was dissected out from coronal sections of P14 and adult brains, and dissociated single cells were subjected to scRNA-seq using the 10x Genomics platform. From two independent experiments for both stages, transcriptome data with a median of ∼3000 genes/cell were obtained from a total of 17,941 and 19,505 cells from the adult and P14 SVZs, respectively. Unsupervised cell clustering was performed by the Louvain algorithm together with dimension reduction using the Python implementation of uniform manifold approximation and projection (UMAP) using the top 18 significant principal components determined by JackStraw plot (Becht et al., 2018). Such clustering identified 17 and 14 distinct cell groups in the adult and P14 cells, respectively, based on their transcriptome signatures (Fig. 2A,B; Table S1). As expected, a large number of Olig2-expressing cells belonged to OL clusters (blue outlines in Fig. 2A,B), including oligodendrocyte progenitor cells (OPCs), pre-oligodendrocytes (Pre-OLs), and mature OLs at both stages (Fig. 2C,E,G,I). By contrast, fewer Gsx2-expressing cells were detected in these OL clusters (Fig. 2D,F,G,I). Moreover, numerous Olig2-expressing cells were detected in the NSC lineage clusters (red outlines in Fig. 2A,B), and their numbers were comparable to those of Gsx2-expressing cells (Fig. 2C-I). For example, 13.9% and 8.0% of cells in the adult NSC lineage expressed Olig2 and Gsx2 transcripts, respectively, whereas 17.1% and 15.9% were Olig2$^+$ and Gsx2$^+$, respectively, in the P14 SVZ (Fig. 2G,I). Furthermore, within the aNSC/TAP cell cluster (clusters 4 and 1 for adult and P14 SVZs, respectively), Olig2$^+$ and Gsx2$^+$ cells corresponded to 24.1% and 29.9% in adult animals and 37.2% and 34.1% in P14 animals, respectively. These results reiterate the aforementioned histological finding that both Olig2- and Gsx2-expressing cells are major populations among postnatal NSCs. We also identified the occurrence of Olig2-expressing NSCs in previously reported scRNA-seq datasets (Coré et al., 2020; Cebrian-Silla et al., 2021). Interestingly, approximately one-third of Olig2$^+$ and Gsx2$^+$ aNSCs/TAPs co-expressed Olig2 and Gsx2 transcripts (Fig. 2G,I). Such results appear to be contradictory to the aforementioned results that Olig2 and Gsx2 proteins are mostly expressed in distinct cells. However, further analysis demonstrated that cells expressing Olig2 transcripts at high levels contained Gsx2 transcripts mostly at a low level, whereas cells with many Gsx2 transcripts mainly expressed only a few Olig2 transcripts (Fig. 2H,J). Thus, cells with high copy numbers of Olig2 and Gsx2 transcripts were mostly mutually exclusive, similar to the protein expression results. These results suggest that the expression of Olig2 and Gsx2 proteins in NSCs is regulated by both transcriptional and post-transcriptional mechanisms, as demonstrated in previous studies for embryonic NSCs (Shibata et al., 2011; de Chevigny et al., 2012).

Development (2022) 149, dev200028. doi:10.1242/dev.200028

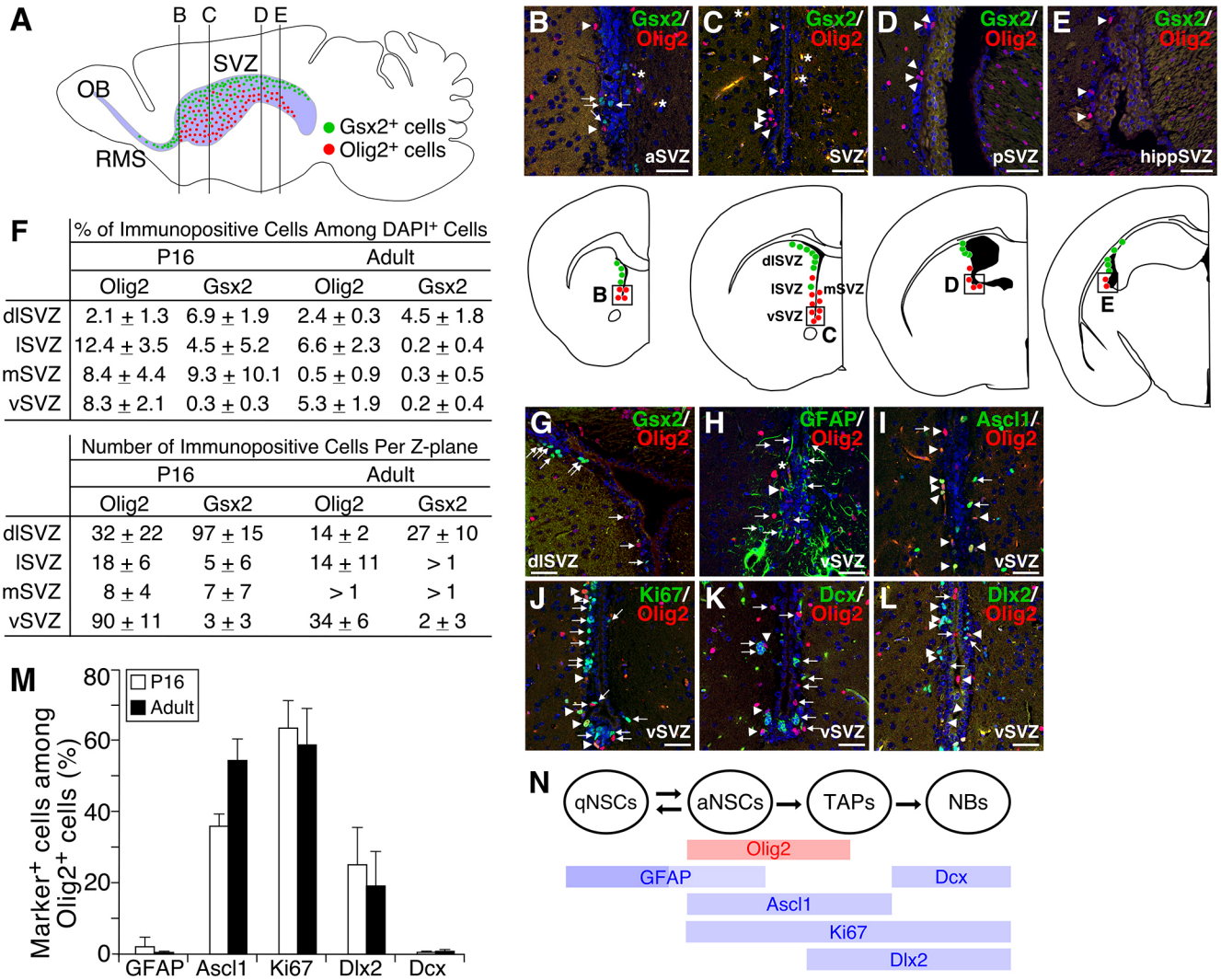

F

	% of Immunopositive Cells Among DAPI+ Cells			
	P16		Adult	
	Olig2	Gsx2	Olig2	Gsx2
dlSVZ	2.1 ± 1.3	6.9 ± 1.9	2.4 ± 0.3	4.5 ± 1.8
lSVZ	12.4 ± 3.5	4.5 ± 5.2	6.6 ± 2.3	0.2 ± 0.4
mSVZ	8.4 ± 4.4	9.3 ± 10.1	0.5 ± 0.9	0.3 ± 0.5
vSVZ	8.3 ± 2.1	0.3 ± 0.3	5.3 ± 1.9	0.2 ± 0.4

	Number of Immunopositive Cells Per Z-plane			
	P16		Adult	
	Olig2	Gsx2	Olig2	Gsx2
dlSVZ	32 ± 22	97 ± 15	14 ± 2	27 ± 10
lSVZ	18 ± 6	5 ± 6	14 ± 11	>1
mSVZ	8 ± 4	7 ± 7	>1	>1
vSVZ	90 ± 11	3 ± 3	34 ± 6	2 ± 3

Fig. 1. Expression of Olig2 in the early postnatal and adult SVZ. (A-E) The distribution of Olig2$^+$ cells in the adult stem cell niche. (A) Schematic of the distribution patterns of Olig2$^+$ (red dots) and Gsx2$^+$ (green dots) cells in the lateral wall of the LV. Vertical lines indicate the approximate locations of the coronal planes in B-E. (B-E) Representative single *z*-plane confocal images of the vSVZ (optical resolution of 0.325 µm) stained for Olig2 (red, arrowheads) and Gsx2 (green, arrows) at different AP levels (aSVZ, anterior SVZ; SVZ, typical, dorsoventrally elongated SVZ; pSVZ, posterior SVZ adjacent to the hippocampal fissure; HippSVZ, posterior SVZ adjacent to the anterodorsal hippocampus). Asterisks indicate nonspecific fluorescent signals. The anterior and posterior ends of the SVZ exist beyond the regions shown in B and E, respectively. Schematics in B-E show the distribution patterns of Olig2$^+$ (red dots) and Gsx2$^+$ (green dots) cells along the LV. Boxes indicate the approximate locations of the photographs in the upper panels. The locations of distinct SVZ subdomains are indicated in the lower panel in C. Olig2$^+$ and Gsx2$^+$ cells coexist in the ventral aspect of the aSVZ (B), but not in more posterior SVZs (C-E). (F) Percentage distribution of Olig2$^+$ and Gsx2$^+$ cells among total DAPI$^+$ cells (upper panel) and the number of Olig2$^+$ and Gsx2$^+$ cells in a single confocal *z*-plane (lower panel) in various subdomains of the typical SVZ in the P16 and adult brain (data are mean±s.d., *n*=3 for each stage). (G) Mutually exclusive expression of Olig2 (red) and Gsx2 (green, arrows) in the dlSVZ. (H-L) Representative images of Olig2$^+$ cells (red) co-stained for various cell type markers (green) in the vSVZ in the adult brain. Arrowheads and arrows indicate co-expressing and single-positive cells, respectively. (M) The percentages of Olig2$^+$ cells co-expressing Gfap, Ascl1, Ki67, Dlx2 and Dcx in the vSVZ of adult (filled bars) and P16 (open bars) brains (data are mean±s.d., *n*=3). (N) Schematic of the expression patterns of Olig2 and other molecular markers in various cell types in the stem cell lineage. Scale bars: 50 µm in B-E,G-L.

Olig2-expressing adult NSCs continuously generate new olfactory bulb neurons

We next examined the fate of Olig2-expressing NSCs in the adult SVZ. We took advantage of the Cre/LoxP lineage-tracing strategy using *Olig2-CreER* mice, in which *CreER* cDNA was knocked into the endogenous *Olig2* locus (Takebayashi et al., 2002). Adult mice carrying *Olig2*$^{CreER/+}$*;Rosa-tdTomato*$^{+/-}$ or $^{+/+}$ were treated with the CreER activator tamoxifen (Tx) once daily for 2 and 10 days and analyzed 3 and 56 days after the first Tx treatment, respectively (hereafter, D3 and D56) (Madisen et al., 2010). To detect adult-born neurons, D56 animals also received intraperitoneal injections of 5-bromo-2′-deoxyuridine (BrdU) twice a day for 5 days 3 weeks prior to histological analysis (from D35 to D39). In these animals, recombined Olig2-expressing NSCs and their progeny were detected as *Rosa-tdTomato*-expressing (tdTomato$^+$) cells.

In *Olig2-CreER* mice at D3, all tdTomato$^+$ cells detected in the SVZ co-expressed Olig2 as expected (62 cells examined in two animals). However, in D56 animals, only approximately a half of tdTomato$^+$ cells expressed Olig2 in the SVZ (Fig. 3A,G). Thus, a significant fraction of the fate-mapped cells lost Olig2 expression between D3 and D56. Moreover, approximately 8% and 15% of tdTomato$^+$ cells expressed Ascl1 and Ki67, respectively, at D56,

Development (2022) 149, dev200028. doi:10.1242/dev.200028

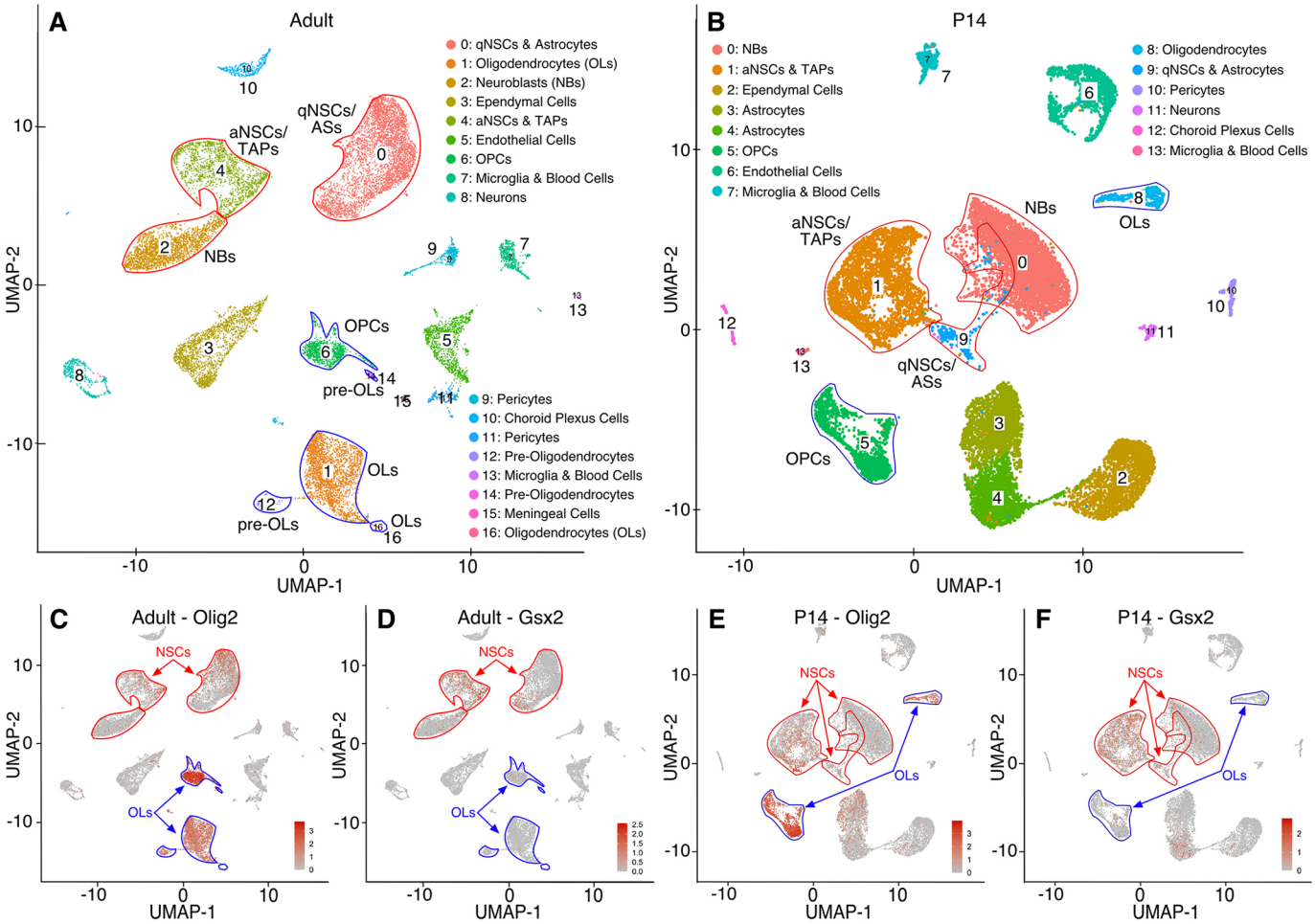

G

Adult	Cell Type	Number	%
NSC Lineage (0+2+4)		8317	
	Olig2$^+$ Cells	1152	13.9
	Gsx2$^+$ Cells	665	8.0
aNSCs/TAPs (4)		1720	
	Total Olig2$^+$ cells	414	24.1
	Total Gsx2$^+$ Cells	514	29.9
	Olig2$^+$/Gsx2$^+$ Cells	139	8.1
	Olig2$^+$ Only Cells	275	16.0
	Gsx2$^+$ Only Cells	375	21.8
Oligodendrocytes (1+6+12+14+16)		4090	
	Olig2$^+$ Cells	3262	79.8
	Gsx2$^+$ Cells	39	1.0

H

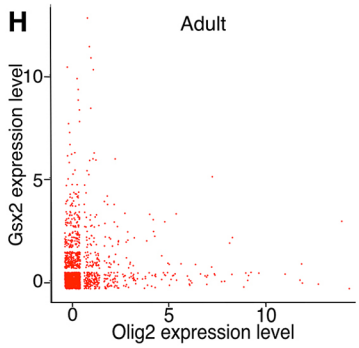

I

P14	Cell Type	Number	%
NSC Lineage (0+1+9)		8510	
	Olig2$^+$ Cells	1457	17.1
	Gsx2$^+$ Cells	1355	15.9
aNSCs/TAPs (1)		3354	
	Total Olig2$^+$ cells	1249	37.2
	Total Gsx2$^+$ Cells	1144	34.1
	Olig2$^+$/Gsx2$^+$ Cells	419	12.5
	Olig2$^+$ Only Cells	830	24.7
	Gsx2$^+$ Only Cells	725	21.6
Oligodendrocytes (5+8)		2134	
	Olig2$^+$ Cells	2058	96.4
	Gsx2$^+$ Cells	88	4.1

J

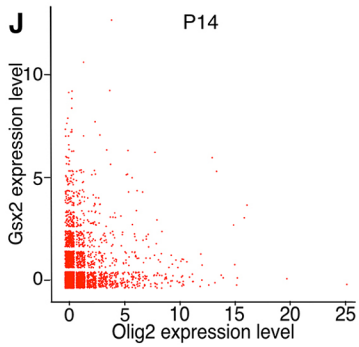

Fig. 2. See next page for legend.

Development (2022) 149, dev200028. doi:10.1242/dev.200028

Fig. 2. scRNA-seq analysis of Olig2-expressing NSCs in the adult and P14 brain. (A,B) UMAP plots of distinct cell types in the SVZ and adjacent regions of the adult (A) and P14 (B) brain. Seventeen and 14 molecularly distinct cell types were identified in adult and P14 tissues, respectively. The cell type of each cluster was identified based on the overall profile of genes with enriched expression (Table S1). Clusters with characteristics of cells in the NSC (clusters 0, 2 and 4 in A, and clusters 0, 1 and 9 in B) and OL lineages (clusters 1, 6, 12, 14 and 16 in A, and clusters 5 and 8 in B) are indicated in red and blue outlines, respectively. (C-F) Feature plots of cells expressing Olig2 (C,E) and Gsx2 (D,F) (red dots) among distinct cell clusters in the adult (C,D) and P14 (E,F) brain. Clusters of cells in the NSC and OL lineages are indicated by red and blue outlines, respectively. (G-J) Expression of Olig2 and Gsx2 in NSC and OL lineages. (G,I) Numbers of cells expressing Olig2 and Gsx2 either alone or in combination in the NSC and OL lineages in adult (G) and P14 (I) brain. (H,J) Dot plots of the relative expression levels of Olig2 and Gsx2 transcripts in individual aNSCs/TAPs (clusters 4 and 1 in the adult and P14 SVZs, respectively) (Pearson's correlation coefficient: H, −0.85; I, −0.84). The number of red dots in each square corresponds to the number of cells in which the indicated normalized copy numbers of Olig2 and Gsx2 transcripts were detected.

indicating that tdTomato-labeled Olig2$^+$ NSCs keep proliferating and generating aNSCs and TAPs during this 8-week period (Fig. 3B,C,G). In addition, many tdTomato$^+$ cells also co-expressed Dlx2, Dcx and Pax6, which mark mainly late TAPs and NBs (Fig. 3D-G) (Kohwi et al., 2005; Brill et al., 2008; de Chevigny et al., 2012). Thus, tdTomato$^+$ cells derived from Olig2$^+$ cells include not only NSCs, but also TAPs and NBs, the two major progeny of NSCs in *Olig2-CreER* mice at D56.

We next examined the OB of *Olig2-CreER* mice. Only a few tdTomato$^+$ cells were detected in D3 mice, and most of these were Olig2$^+$ with typical OL morphology (among more than 60 cells examined). However, we found numerous tdTomato$^+$ cells, corresponding to ∼4% of all 4′,6-diamidino-2-phenylindole (DAPI)$^+$ cells (4.1±0.5%, n=3 animals), in the OB of *Olig2-CreER* mice at D56 (Fig. 3H-J). Olig2 is expressed in OLs and astrocytes but not in neurons in the adult OB (Wang et al., 2021). Consistent with this, ∼40% of tdTomato$^+$ cells in the OB expressed Olig2 and Olig1 (Fig. 3K-K″,L-L″,P). These tdTomato$^+$ OLs were either pre-existing resident OLs or those that were newly generated by NSCs in the SVZ and had subsequently migrated to the OB (Hack et al., 2005; Menn et al., 2006; Ortega et al., 2013). Importantly, however, we found that ∼60% of tdTomato$^+$ cells in the OB were negative for Olig2 or Olig1 (Fig. 3P). These Olig2-negative tdTomato$^+$ cells were most likely to be newborn neurons generated by Olig2$^+$ NSCs. In fact, we found that ∼40% of tdTomato$^+$ cells across multiple layers co-expressed Dlx2 and NeuN (Fig. 3M-N″,P). In particular, ∼60% of tdTomato$^+$ cells in the granule cell layer (GCL) were Dlx2$^+$ and NeuN$^+$ neurons (Fig. 3P). By contrast, because many neurons in the glomerular layer (GL) and plexiform layer (PL: external and internal plexiform layers combined with the mitral cell layer in the middle) remain immuno-negative for Dlx2 or

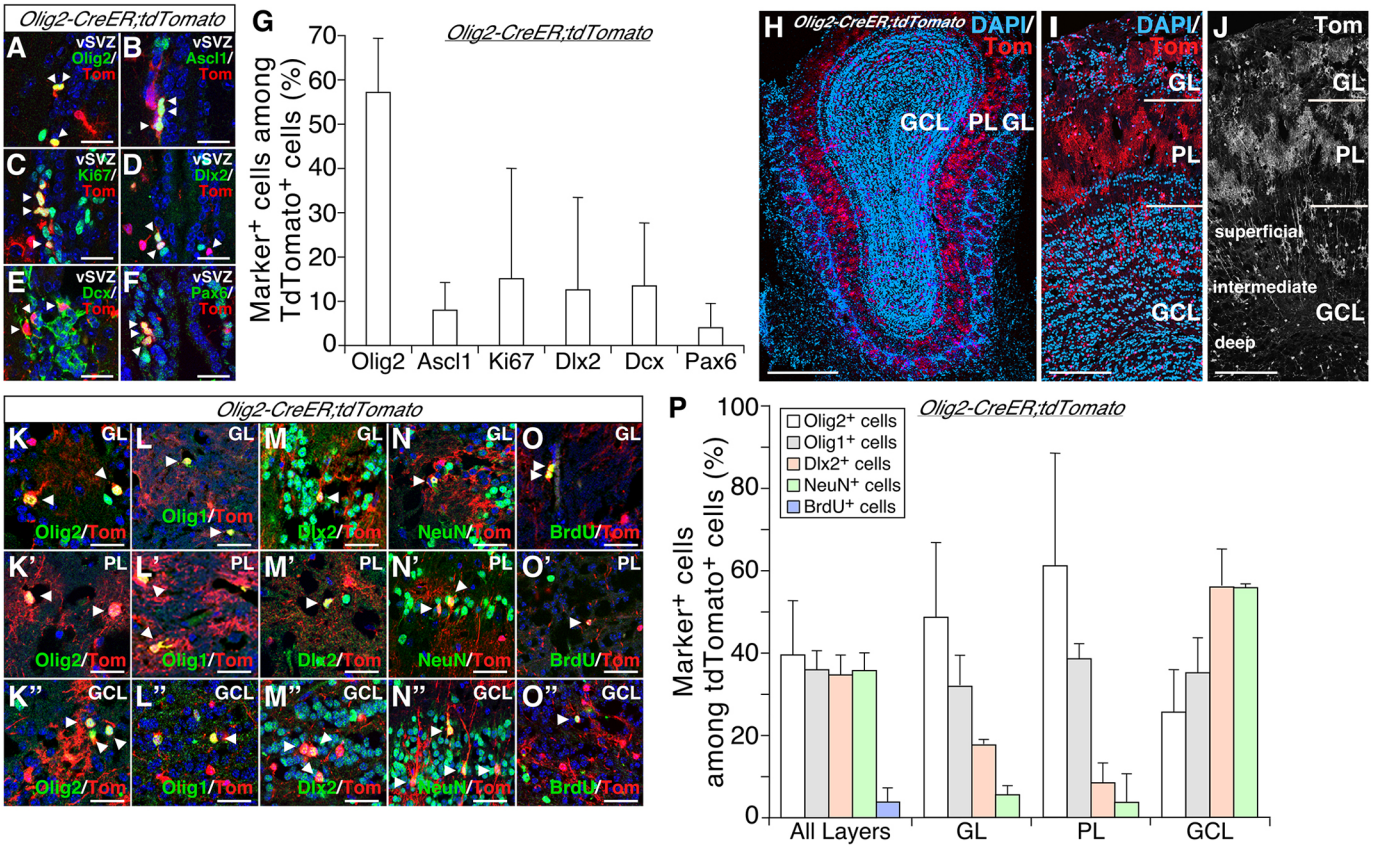

Fig. 3. Lineage tracing of Olig2$^+$ NSCs and their neuronal progeny in the adult OB. (A-F) Representative images of tdTomato$^+$ fate-mapped cells co-expressing various cell type markers in the vSVZ of adult *Olig2-CreER* mice at D56. Co-expressing cells are indicated by arrowheads. (G) Percentages of tdTomato$^+$ cells co-expressing Olig2, Ascl1, Ki67, Dlx2, Dcx and Pax6 in the vSVZ at D56 (data are mean±s.d., n=4 animals). (H,I) Representative images of tdTomato$^+$ cells (red; co-stained with DAPI in blue) in a coronal section of the whole OB and a higher magnification view, respectively.(J) Gray-scale image of I without DAPI signals for better visualization of tdTomato$^+$ cells in various OB layers. (K-O″) Representative images of tdTomato$^+$ cells (red) co-expressing various markers (green) (indicated by arrowheads) in the GL (K-O), PL (K′-O′), and GCL (K″-O″). (P) Percentages of tdTomato$^+$ fate-mapped cells co-expressing various markers in different OB layers at D56 (data are mean±s.d., n=3). Scale bars: 25 µm in A-F,K-O″; 500 µm in H; 200 µm in I,J.

Development (2022) 149, dev200028. doi:10.1242/dev.200028

NeuN even at mature stages (Parrish-Aungst et al., 2007; Long et al., 2007), the percent overlaps between tdTomato and these neuronal markers in these layers were lower than in the GCL (Fig. 3P). Moreover, a small but significant fraction of tdTomato$^+$ cells became BrdU$^+$ 3 weeks after the animals received BrdU (Fig. 3O-O″,P). Together, these results demonstrate that Olig2-expressing NSCs at the adult stage generate new neurons that migrate to the OB.

Olig2$^+$ NSCs generate multiple subtypes of neuron in the adult OB

We next examined the subtype identity of neurons generated by Olig2$^+$ NSCs. After excluding Olig2$^+$ OLs from the total tdTomato$^+$ cells, ∼60% of *Olig2-CreER* fate-mapped cells belonged to the GCL, whereas 30% and 10% were detected in the GL and PL, respectively (Fig. 4A). Thus, Olig2$^+$ NSCs generate new neurons in multiple layers of the OB. In the GL, neurons expressing calretinin (CR), neurocalcin (NC), calbindin (CB), tyrosine hydroxylase (TH) and parvalbumin (PV) represent discrete interneuron populations, except for a partial overlap of CR$^+$ (∼15%) and PV$^+$ (∼20%) cells with NC$^+$ cells (Briñón et al., 1999; Parrish-Aungst et al., 2007). We found that significant fractions of tdTomato$^+$ cells in the GL expressed CR, NC and TH, but no tdTomato$^+$ cells were CB$^+$ or PV$^+$ (Fig. 4B-F,K). A small fraction of tdTomato$^+$ cells in the PL and GCL also co-expressed CR (Fig. 4G,J,K). Given that adult-born OB neurons require a long time period (6-8 weeks) after their birth to express mature subtype markers fully (Kohwi et al., 2007), it is likely that more tdTomato$^+$ cells would express subtype-specific markers if analyzed at later time points. In fact, ∼40% of tdTomato$^+$ cells expressed the homeodomain TF Pax6 in the GL and GCL, and ∼25% express the MADS box TF Mef2c in the GCL (Fig. 4H,I,L) (Lyons et al., 1995; Hack et al., 2005; Kohwi et al., 2005; Brill et al., 2008). These results demonstrate that Olig2$^+$ NSCs generate multiple neuronal subtypes across all layers in the adult OB.

Developmental changes in the molecular properties of Olig2-expressing NSCs/progenitors

The aforementioned results demonstrated that Olig2-expressing NSCs in the adult SVZ generate new OB neurons. Previous studies have also shown that Olig2$^+$ NSCs/progenitors continuously produce new neurons and glia from early to late embryonic stages

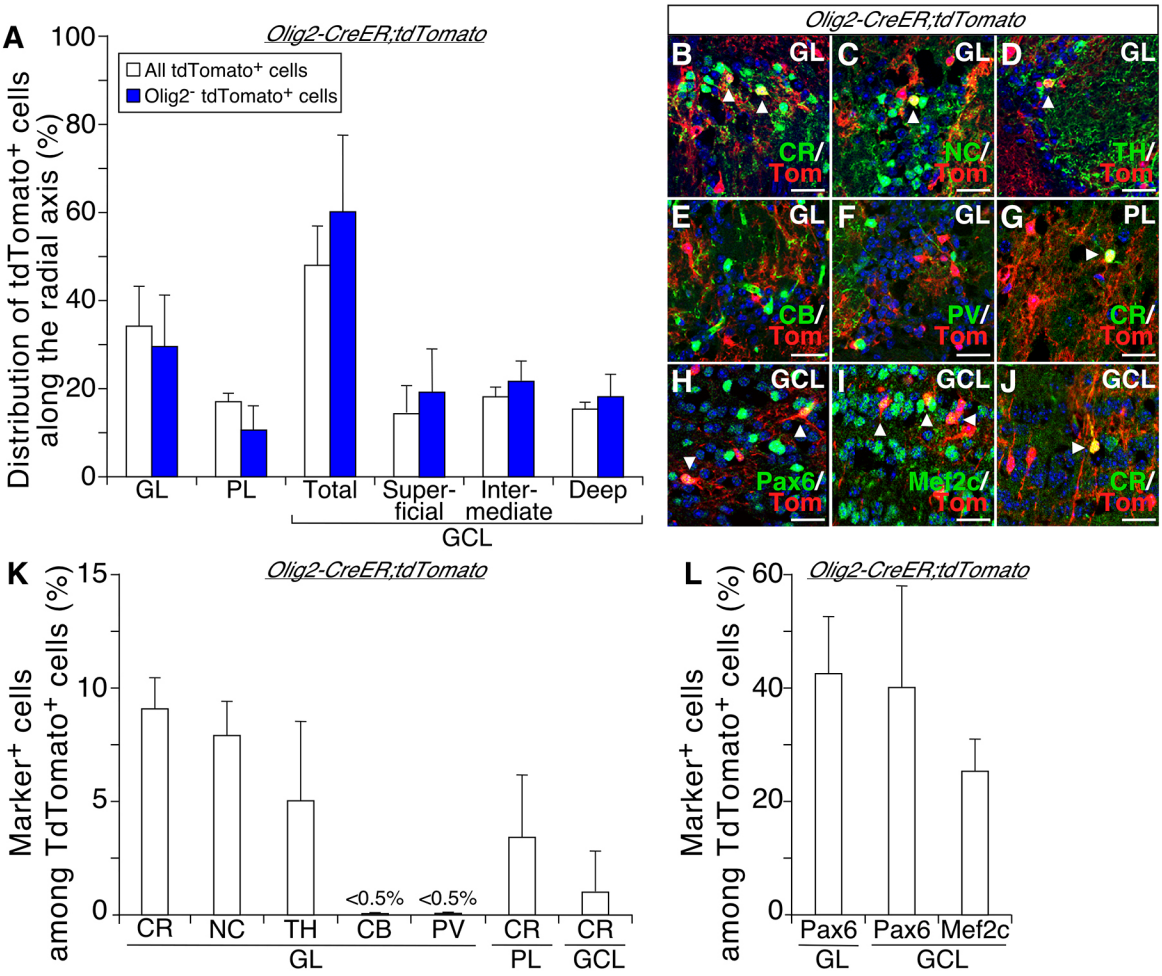

Fig. 4. Olig2$^+$ NSCs generate a variety of neuronal subtypes in the adult OB. (A) Laminar distribution pattern of tdTomato$^+$ cells at D56 showing the percentages of tdTomato$^+$ cells in the GL, PL and the whole GCL, as well as the superficial, intermediate and deep sublayers of the GCL in adult *Olig2-CreER* mice at D56. Open bars represent data on all tdTomato$^+$ cells, whereas blue bars represent data on tdTomato$^+$ cells excluding Olig2$^+$ OLs, which correspond to Olig2$^+$ NSC-derived new neurons (data are mean±s.d., *n*=3). (B-J) Representative images of tdTomato$^+$ cells (red) co-expressing respective markers (arrowheads) in the GL (B-F), PL (G) and GCL (H-J) of the OB in *Olig2-CreER* mice at D56. (K,L) Percentages of tdTomato$^+$ cells co-expressing various neuronal subtype markers (K) and TFs (L) at D56. The layers and neuronal subtype markers examined are detailed below the *x*-axis (data are mean±s.d., *n*=3). Scale bars: 25 µm in B-J.

Development (2022) 149, dev200028. doi:10.1242/dev.200028

(Miyoshi et al., 2007; Ono et al., 2008). Thus, we next sought to interrogate how the molecular properties of Olig2$^+$ NSCs/progenitors change over time by comparing their transcriptome profiles. We obtained scRNA-seq data on the whole ventral telencephalon at embryonic day (E) 12.5 and E18.5 using the 10x Genomics platform and compared these datasets with those from P14 and adult SVZ. First, cells that belonged to NSC/progenitor clusters (qNSC/astrocyte and aNSC/TAP) at each stage were identified based on their transcriptome profiles, and Olig2-expressing cells within these clusters were isolated (Fig. S1 and Table S1). Subsequently, these cells were combined and subjected to reclustering using UMAP plots. In these plots, the physical distance between individual cells reflects the extent of the similarity of their transcriptome profiles, unlike conventional tSNE analysis, so that one can visualize the overall similarities and differences between cells at different stages (Becht et al., 2018). Such an analysis revealed that Olig2$^+$ NSCs/progenitors at different stages as a whole exhibited clearly distinct transcriptome profiles (Fig. 5A-C; Table S2) and were divided into partially overlapping, but clearly distinct, subclusters (Fig. 5D,E; Table S3). For example, Olig2$^+$ NSCs/progenitors at E12.5 and E18.5 (green and blue dots, respectively, in Fig. 5A,B) were divided into four (0, 1, 3 and 5) and three (3, 4 and 7) distinct subclusters, respectively (compare Fig. 5D with Fig. 5A,B) (Haubensak et al., 2004; Noctor et al., 2004; Fish et al., 2008; Wilsch-Bräuninger et al., 2016). Among these subclusters, subcluster 3 was the only population shared between E12.5 and E18.5 (Fig. 5D). Transcriptome profiling further indicated that cells in subcluster 7 showed enriched expression of many genes related to glial progenitors and immature astrocytes, such as vimentin (*Vim*), solute carrier family 1 member 3 (*Slc1a3* or GLAST), fatty acid-binding protein 7 (*Fabp7* or *Blbp*) and aldehyde dehydrogenase 1 family member L1 (*Aldh1l1*) (Fig. 5E; Table S3). The occurrence of these unique cells at E18.5 is consistent with the fact that Olig2$^+$ progenitors at late embryonic stages generate not only neurons, but also astrocytes and OLs (Miyoshi et al., 2007; Ono et al., 2008). Moreover, the majority of cells remaining at E18.5 formed subcluster 4, which showed enriched expression of genes related to basal progenitors, such as *Ascl1*, *Dlx1*/*2*, and *Sox4*, but their overall transcriptome profile was clearly distinguishable from the basal progenitor subcluster at E12.5 (subcluster 3) (Fig. 5D,E). Thus, the properties of Olig2$^+$ progenitors at E18.5 are molecularly distinct from those at E12.5.

Clusters of postnatal Olig2$^+$ cells also partially overlapped with E18.5 cells, but the majority belonged to discrete clusters with very different transcriptome profiles (Fig. 5A-C). The majority of P14 cells belonged to a single cluster (subcluster 2 in Fig. 5D), and their transcriptome signature was reminiscent of the properties of aNSCs and TAPs (Fig. 5E; Table S3). This gene expression signature of P14 cells reflects a higher neurogenic activity of NSCs at early postnatal stages than during the adult stage (Batista-Brito et al., 2008; Sakamoto et al., 2014). By contrast, a significant fraction of cells at the adult stage formed a unique cluster (subcluster 6 in Fig. 5D), characterized by the enriched expression of genes related to qNSCs and astrocytes, such as retinoid-related orphan receptor beta (*Rorb*), solute carrier family 1 member 2 (*Slc1a2* or *Eaat2*) and gap junction protein alpha 1 (*Gja1*) (Fig. 5E; Table S3). The occurrence of this adult-specific subcluster is consistent with the fact that, while NSCs mature postnatally, their neurogenic activity gradually declines, and the majority become quiescent or divide only slowly (Götz et al., 2016).

The cell cycle profile also revealed distinct properties of Olig2$^+$ NSCs/progenitors at different stages. Based on the relative expression levels of a set of cell cycle phase-specific genes (Table S4), individual cells could be divided into three groups: cells in the G0/G1, S and G2/M phases (Fig. 5F,G). This analysis demonstrates that more than 90% of Olig2$^+$ NSCs/progenitors at E12.5 were either in the S or G2/M phase (Fig. 5G), and that the transcriptome profile of cells in the G0/G1 phase (red dots) more closely resembles cells in the S phase (blue dots) than those in the G2/M phase (green dots) (Fig. 5F). By contrast, among Olig2$^+$ NSCs/progenitors at E18.5, there were fewer cells in the S phase, and ∼35% of cells were in the G0/G1 phase (Fig. 5G). These G0/G1 phase cells were mostly found in the cluster of glial progenitors/immature astrocytes (subcluster 7), reflecting active gliogenesis at late embryonic stages (compare Fig. 5D with Fig. 5F). Postnatally, cells in the G0/G1 phase further increased and reached 72% at the adult stage (Fig. 5G). Moreover, subcluster 2, which corresponds to aNSCs/TAPs in the P14 and adult SVZ, is a mixture of cells in all phases of the cell cycle, whereas subcluster 6, which contains adult qNSCs and astrocytes, mainly comprised cells in the G0/G1 phase (Fig. 5F). These results clearly demonstrate a stage-dependent stepwise decline in overall proliferative activity during the postnatal development of NSCs.

Comparisons of transcriptome profiles related to various metabolic and signaling pathways by ReactomeGSA also revealed significant stage-dependent changes (https://reactome.org; Griss et al., 2020). A gene set variation analysis (GSVA) of genes associated with specific metabolic and signaling pathways was performed using datasets from all four stages, and the relative activity of each pathway was scored and compared as described in a previous study (Hänzelmann et al., 2013) (for details, see Materials and Methods and Table S5). We found that the activity of many pathways increased over time from E12.5 to adult stages, but the timing of their increase varied significantly. For example, the activity of the signaling pathways for the neurotrophin receptors TrkA and TrkB was low in cells at E12.5 but showed gradual increases from E18.5 to the adult stage (blue font in Fig. 5H). By contrast, the activity of various lipid metabolism and neurotransmission/ion transport-related pathways (red and green fonts, respectively, in Fig. 5H) remained very low during embryogenesis, but those pathways became significantly active at P14 and reached higher levels at the adult stage. These changes probably reflect that NSCs/progenitors at postnatal stages gradually acquire responsiveness to various local and systemic environmental cues (Nakafuku and Grande, 2020). Altogether, these results demonstrate that the properties of Olig2$^+$ NSCs/progenitors markedly change over time from early embryonic to adult stages.

Crosstalk between Olig2 and Gsx2 in embryonic and adult NSCs/progenitors

In the developing telencephalon, both Olig2 and Gsx2 are expressed in broad progenitor domains, including the lateral ganglionic eminence (LGE), medial ganglionic eminence (MGE), preoptic area (POA) and septum (Toresson et al., 2000; Toresson and Campbell, 2001; Yun et al., 2001, 2003; Takebayashi et al., 2002; Petryniak et al., 2007; Wang et al., 2013; Chapman et al., 2013, 2018). In particular, Gsx2 expression is initially broad and uniform at early stages (E9.5-E11.5), but subsequently becomes refined to a high dorsal-low ventral gradient within the LGE from E12.5 onward (Stenman et al., 2003; Waclaw et al., 2009). Thus, the Gsx2-high and Olig2-high progenitor domains become mostly complementary to each other at late embryonic stages (Chapman et al., 2018). Such complementary patterns are reminiscent of their expression in the postnatal SVZ described above.

Development (2022) 149, dev200028. doi:10.1242/dev.200028

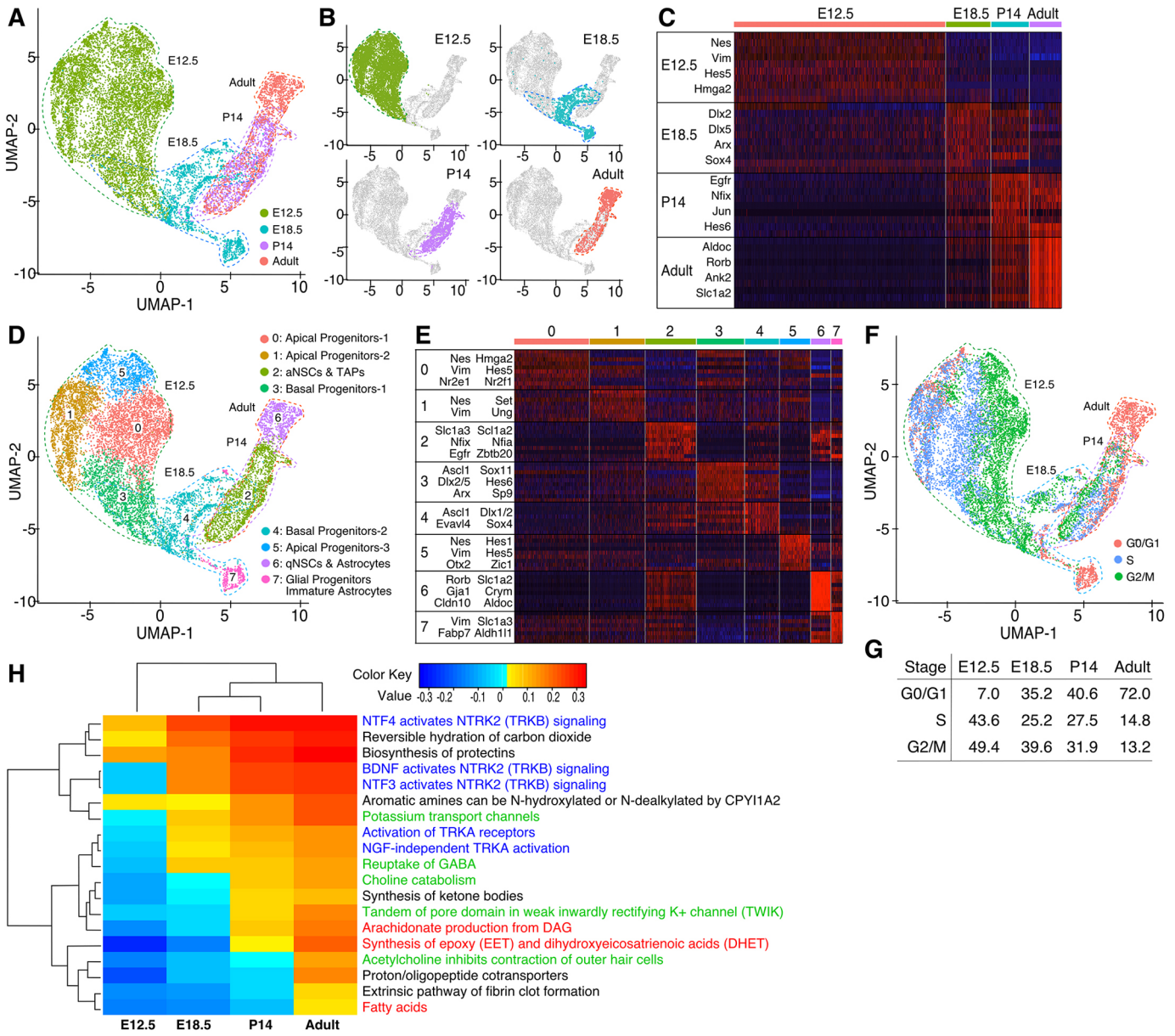

Stage	E12.5	E18.5	P14	Adult
G0/G1	7.0	35.2	40.6	72.0
S	43.6	25.2	27.5	14.8
G2/M	49.4	39.6	31.9	13.2

Fig. 5. Developmental changes in the molecular properties of Olig2$^+$ NSCs revealed by scRNA-seq. (A,B) UMAP clustering of Olig2$^+$ NSCs/progenitors from different developmental stages. Cells from E12.5 (green dots), E18.5 (blue dots), P14 (purple dots) and adult (orange dots) stages were combined and reclustered to visualize their similarities and differences. (A) Cells from all stages combined; (B) cells at each stage shown separately by overlaying on top of all cells (gray dots). (C) Heatmap visualization of distinct transcriptome profiles of Olig2$^+$ NSCs/progenitors at different stages. The relative expression levels of enriched genes (top ten genes for E12.5, E18.5 and adult stages, and top nine genes for P14) in cells at each stage (shown at the top) are compared, and representative genes are listed in the left column (Table S2). (D) UMAP clustering of Olig2$^+$ NSCs/progenitors from all four stages into eight distinct subclusters. Each subcluster in D is named based on the similarity of its overall transcriptome profile with known progenitor subtypes. (E) Heatmap of the relative expression levels of eight to ten enriched genes in each subcluster (shown at the top); representative genes in each subcluster are listed in the left column (Table S3). (F,G) Cell cycle profiles of Olig2$^+$ NSCs/progenitors at different stages. (F) Feature plot of cells in distinct cell cycle phases among subclusters of Olig2$^+$ NSCs/progenitors. (G) Percentages of cells in the G0/G1 (orange dots), S (blue dots) and G2/M (green dots) phases among total cells at each stage. For the list of genes enriched in S and G2/M phases, see Table S4. (H) Heatmap comparison of the activity of various molecular pathways in Olig2$^+$ NSCs/progenitors at different stages. The top 19 molecular pathways that showed the largest differences in activity level among cells at different stages are compared. Pathways related to neurotrophin signaling, lipid metabolism and neurotransmission/ion transport are highlighted in blue, red and green font, respectively.

Importantly, our recent study demonstrated that the dorsal limit of Olig2 expression in the developing LGE expands in *Gsx2* mutant embryos (Chapman et al., 2018). Thus, cross-repression between Olig2 and Gsx2 may play an important role in establishing and/or maintaining their mutual expression patterns. To address this possibility, we compared the expression of Olig2 and Gsx2 in both *Gsx2* and *Olig2* germline mutant embryos at E15.5. In control embryos, the ventral limit of Gsx2-high expression was confined to the dLGE (Fig. 6A, arrow), whereas the dorsal limit of Olig2 expression remained in the ventral half of the vLGE (Fig. 6A, arrowhead). By contrast, Gsx2-high expression expanded far ventrally and reached the MGE in *Olig2* knockout (KO) embryos (Fig. 6B, arrow). Conversely, in *Gsx2* KO embryos, the dorsal limit of Olig2 expression expanded dorsally and reached the ventral limit

Development (2022) 149, dev200028. doi:10.1242/dev.200028

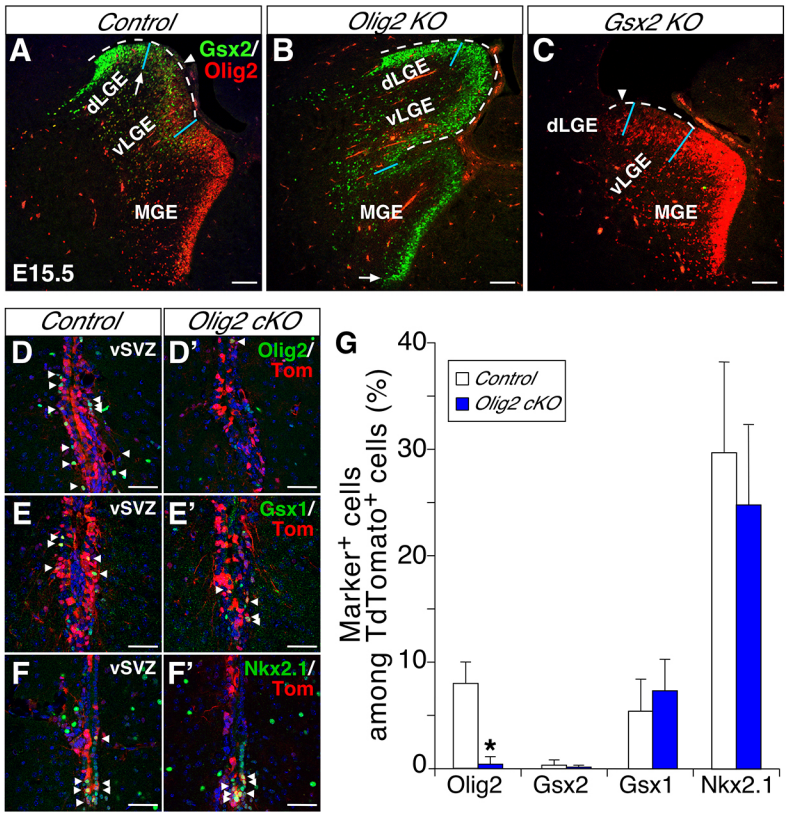

Fig. 6. Cross-repression between Olig2 and Gsx2 in embryonic and adult brains. (A-C) Expression of Olig2 (red) and Gsx2 (green) proteins in progenitor domains of the ventral telencephalon in control (A), *Olig2* KO (B) and *Gsx2* KO (C) embryos at E15.5. Dashed-white lines indicate the ventricular surface of the LGE, and short blue lines indicate the borders between the dLGE, vLGE and MGE. Arrowheads indicate the dorsal limit of Olig2 expression, whereas arrows indicate the ventral limit of Gsx2-high expression. Similar phenotypes were observed in more than three embryos examined for each genotype. (D-G) Impact of conditional inactivation of Olig2 on the region-selective expression of Olig2, Gsx2, Gsx1 and Nkx2.1 in adult NSCs. (D-F′) Representative images of tdTomato$^+$ cells co-expressing the regional identity markers Olig2, Gsx1 and Nkx2.1 (arrowheads) in the vSVZ of control and *Olig2* cKO mice at D28. (G) Percentages of tdTomato$^+$ cells co-expressing various TFs in the vSVZ of control and *Olig2* cKO mice at D28 (data are mean±s.d., n=5 for control and n=4 for cKO animals). For quantification of Nkx2.1$^+$ cells, sections slightly posterior to those for the standard SVZ analysis were used. *P<0.05 compared with control animals (Student's and Welch's t-tests for parametric and nonparametric data, respectively). Scale bars: 50 µm in A-F′.

of the dLGE (Fig. 6C, arrowhead), where both the dLGE and vLGE were markedly reduced in size as a result of *Gsx2* loss (compare dashed lines in Fig. 6A with those in Fig. 6C) (Toresson et al., 2000; Yun et al., 2001). These results demonstrate that Gsx2 limits the expression of Olig2 dorsally, whereas Olig2 limits the high expression of Gsx2 ventrally in embryonic NSCs/progenitors. Whether such mutual cross-repression is attributable to direct transcriptional repression remains to be investigated.

Given that these germline mutant animals die at birth (Toresson et al., 2000; Dessaud et al., 2007), we next used the CreER-loxP system for the conditional inactivation of these genes in adult NSCs. We generated mice homozygous for a floxed allele of *Olig2* (*Olig2^{flox}*) (Yue et al., 2006; Cai et al., 2007) and heterozygous for a *GLAST-CreER* knock-in allele (Mori et al., 2006). The latter contained a CreER transgene expressed from the locus of the glutamate transporter gene *GLAST* so that we were able to evaluate the impact of Olig2 inactivation in the most primitive/undifferentiated GLAST$^+$ NSCs. *Olig2* conditional knockout (cKO) (*Olig2$^{flox/flox}$;GLAST-CreER$^{+/-}$;Rosa-tdTomato$^{+/-}$* or $^{+/+}$) and their littermate control (*Olig2$^{flox/+}$* or $^{+/+}$*;GLAST-CreER$^{+/-}$;Rosa-tdTomato$^{+/-}$* or $^{+/+}$) mice were treated with Tx at the age of 10-12 weeks, and subsequently analyzed at D28. As expected, the percentage of Olig2$^+$ cells among tdTomato$^+$ recombined cells decreased by more than 90% in the vSVZ of *Olig2* cKO mice compared with control animals (Fig. 6D,D′,G). However, in these mice, the dorsally restricted expression pattern of Gsx2 did not significantly change, and the percentages of Gsx2$^+$ cells among tdTomato$^+$ cells in the vSVZ remained very low (Fig. 6G). Two other homeodomain TFs, Nkx2.1 and Gsx1, are also expressed in a subset of NSCs in the vSVZ (López-Juárez et al., 2013; Merkle et al., 2014; Paul et al., 2017). The ventrally enriched expression of these TFs among tdTomato$^+$ cells did not significantly change either (Fig. 6E-G). Thus, the inactivation of Olig2 does not alter the region-specific expression patterns of either Gsx2 or other NSC identity genes. We also previously reported that Olig2 expression in the dlSVZ is not significantly affected by conditional inactivation of Gsx2 in adult NSCs (López-Juárez et al., 2013). Thus, unlike in embryos, cross-repression between Olig2 and Gsx2 does not play a major role in maintaining their region-selective expression patterns in NSCs in the adult stage.

Impact of conditional inactivation of Olig2 in NSCs on neurogenesis and neuronal subtype specification

The aforementioned immunohistochemical and scRNA-seq analyses demonstrated that Olig2$^+$ cells are a predominant (>50%) NSC population in the vSVZ of the adult brain (Fig. 1M and Fig. 2G). Thus, *GLAST-CreER*-based *Olig2* cKO mice allowed us to examine the role of Olig2 in neuronal differentiation of NSCs in the vSVZ. In fact, only a small fraction of tdTomato$^+$ cells expressed Olig2$^+$, whereas many tdTomato$^+$ cells became Dcx$^+$ and Pax6$^+$ NBs in these *Olig2* cKO mice at D28 (Fig. 6G and Fig. 7D-F). Interestingly, the percentages of Ascl1$^+$ aNSCs/TAPs and Ki67$^+$ proliferative cells among tdTomato$^+$ cells were modestly but significantly increased at D28 compared with control animals (1.4- and 1.2-fold for Ascl1 and Ki67, respectively), suggesting that activation and/or proliferation of NSCs/TAPs are moderately stimulated by the loss of Olig2 (Fig. 7B,B′,C,C′,F). Nevertheless, Dcx$^+$/tdTomato$^+$ and Pax6$^+$/tdTomato$^+$ NBs were detected at comparable levels in *Olig2* cKO and control mice, demonstrating that Olig2 inactivation does not significantly affect neuronal output from adult NSCs (Fig. 7D-F). Thus, certain feedback mechanisms may operate to maintain a steady level of NB production despite a slight increase in the activation and/or proliferation of NSCs/TAPs. Moreover, Gfap$^+$/tdTomato$^+$ cells also remained unchanged between *Olig2* cKO and control mice, suggesting that Gfap$^+$ stem cells are maintained in *Olig2* cKO mice (Fig. 7A,A′,F). Together,

Development (2022) 149, dev200028. doi:10.1242/dev.200028

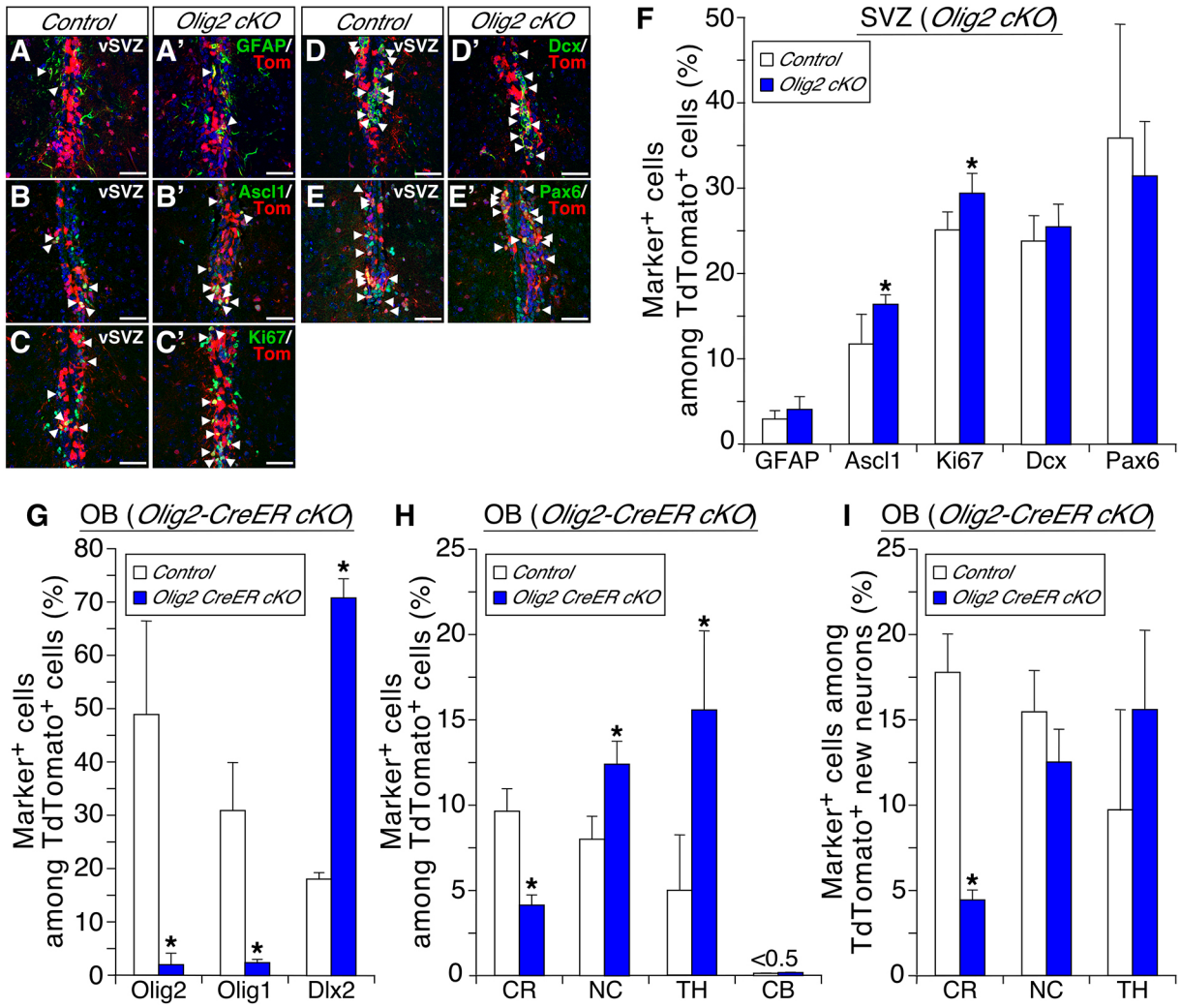

Fig. 7. Impact of conditional inactivation of Olig2 in adult NSCs on neurogenesis and neuronal subtype specification. (A-E′) Representative images of tdTomato$^+$ cells (red) co-expressing various NSC lineage markers (arrowheads) in the vSVZ of control and *Olig2* cKO mice at D28. (F) Percentages of tdTomato$^+$ cells co-expressing Gfap, Ascl1, Ki67, Dcx, and Pax6 in the vSVZ of control and *GLAST-CreER*-based *Olig2* cKO mice at D28 (data are mean±s.d., *n*=5 for control and *n*=4 for cKO animals). (G-I) Percentages of tdTomato$^+$ cells co-expressing Olig2, Olig1 and Dlx2 (G) and various neuronal subtype markers (H,I) in the GL of the OB in control and *Olig2-CreER*-based *Olig2-CreER* cKO mice at D56 (data are mean±s.d., *n*=3). (I) Normalized percentage of cells expressing CR, NC and TH among newborn neurons derived from Olig2$^+$ NSCs (i.e. Olig2-negative tdTomato$^+$ cells). **P* <0.05 compared with control animals (Student's and Welch's *t*-tests for parametric and nonparametric data, respectively). Scale bars: 50 µm in A-E′.

these results demonstrate that Olig2 is dispensable for neurogenesis in adult NSCs.

In these *GLAST-CreER*-based *Olig2* cKO mice, gene recombination and subsequent lineage tracing occurred not only in Olig2$^+$ NSCs, but also in other NSCs, such that tdTomato$^+$ fate-mapped cells derive from heterogeneous NSC populations. Therefore, they are not suitable for examining the impact of Olig2 inactivation on the specificity of neuronal subtypes. For this purpose, we next used *Olig2*$^{CreER/flox}$*;Rosa-tdTomato*$^{+/-}$ or $^{+/+}$ (*Olig2-CreER* cKO) mice, in which Olig2 is inactivated selectively in Olig2$^+$ NSCs. As expected, the percentage of Olig2$^+$ cells among tdTomato$^+$ cells was markedly reduced (by more than 95%) in the GL of the OB in *Olig2-CreER* cKO mice compared with control at D56 (Fig. 7G). In parallel, Olig1$^+$ OLs were markedly reduced among tdTomato$^+$ cells and, conversely, Dlx2$^+$ neurons were dramatically increased and comprised more than 70% of all tdTomato$^+$ cells in the mutant OB (Fig. 7G). Thus, inactivation of Olig2 resulted in a loss of OLs among tdTomato$^+$ cells, and the majority of tdTomato$^+$ cells remaining became neurons in the mutant GL (97.8±2.2% in *Olig2-CreER* cKO mice compared with 51.3±18.2% in control mice, *n*=3). This loss of OLs could be because Olig2 is required for the survival of existing OLs and/or production of new OLs from NSCs.

Importantly, among these remaining tdTomato$^+$ cells in *Olig2-CreER* cKO mice, the percentage of CR$^+$ neurons was reduced by half compared with control animals (Fig. 7H). Furthermore, given that the proportion of new neurons among tdTomato$^+$ cells was doubled in *Olig2* mutants compared with control animals, the percentage of CR$^+$ neurons among new neurons needs to be normalized based on the percentage of Olig2-negative cells among all tdTomato$^+$ cells. Comparison of these normalized values demonstrated that the actual extent of the reduction in CR$^+$ neurons among Olig2$^+$ NSC-derived new neurons (Olig2-negative tdTomato$^+$ cells) was even more drastic (approximately a quarter of the control level) (Fig. 7I). By contrast, although the percentages of NC$^+$ and TH$^+$ cells among all tdTomato$^+$ cells were increased in the

Development (2022) 149, dev200028. doi:10.1242/dev.200028

mutants (Fig. 7H), their normalized fractions among new neurons were comparable between control and mutant mice (Fig. 7I). Given that Olig2 is not expressed in either Dcx$^+$ immature neurons in the SVZ or mature neurons in the OB, it is unlikely that the selective loss of CR$^+$ neurons in the mutant OB results from the defective survival of CR$^+$ neurons. Rather, these results support the idea that Olig2 expression in NSCs is selectively required for the specification of CR$^+$ neurons in the GL.

DISCUSSION

Olig2 reveals molecular heterogeneity of adult NSCs

Our data showed that Olig2-expressing NSCs reside widely along the DV and ML axes of the postnatal SVZ, but that they are most enriched in the ventral subdomain of the SVZ (Fig. 1). Importantly, this ventrally biased distribution pattern of Olig2$^+$ cells is largely complementary to that of dorsally enriched Gsx2-expressing cells in the adult SVZ (López-Juárez et al., 2013). Moreover, Olig2$^+$ and Gsx2$^+$ NSCs were mostly mutually exclusive (Fig. 1). scRNA-seq data also demonstrated that, when combined, Olig2$^+$ and Gsx2$^+$ cells comprised 46% of all aNSCs/TAPs in the adult SVZ and 59% at P14, demonstrating that they are major NSC subtypes in the postnatal brain (Fig. 2). The homeodomain TFs Gsx1 and Nkx2.1, and the zinc finger TF Zic1, are also expressed in a subset of NSCs in the vSVZ and mSVZ, respectively (López-Juárez et al., 2013; Merkle et al., 2014; Paul et al., 2017). However, our data showed that inactivation of Olig2 does not significantly change the expression of these TFs in the vSVZ, Thus, the relationships of these NSCs with Olig2$^+$ and Gsx2$^+$ NSCs are currently unknown and remain to be further investigated.

Crosstalk between Olig2 and Gsx2 in embryonic and adult NSCs

The region-selective expression of Olig2 and Gsx2 defines a similar topological organization of NSC/progenitor domains in embryos and adults. Nevertheless, we found a clear difference in the relationship between Olig2 and Gsx2 in embryonic and adult NSCs. In embryos, genetic inactivation of *Olig2* led to a marked ventral expansion of the Gsx2-high region, whereas inactivation of *Gsx2* resulted in expansion of the dorsal limit of Olig2 expression (Fig. 6). Thus, the border between Gsx2-high and Olig2$^+$ domains is established and/or maintained by cross-repression during embryogenesis. By contrast, conditional inactivation of *Olig2* and *Gsx2* in adult NSCs did not significantly alter the expression of the other gene (this study and López-Juárez et al., 2013). It could be that, once the mutually exclusive expression patterns of Olig2 and Gsx2 are established during embryogenesis, their expression is subsequently maintained independently by certain cell-autonomous mechanisms in the postnatal brain.

Role of Olig2-expressing NSCs in OB interneuron diversity and neurogenesis

Our results demonstrated that Olig2$^+$ adult NSCs contribute to the generation of both CR$^+$ and TH$^+$ neurons in the GL, which are mutually exclusive and the predominant neuronal subtypes among adult-born GL neurons (Lemasson et al., 2005; Kohwi et al., 2007; Batista-Brito et al., 2008; Sakamoto et al., 2014). Our data showed that Olig2$^+$ NSCs were present in all SVZ subdomains, although they were most enriched in the vSVZ. Thus, it is possible that Olig2$^+$ NSCs are heterogeneous and that those in distinct subdomains may be responsible for the generation of distinct neuronal subtypes. Interestingly, it has been proposed that CR$^+$, TH$^+$ and CB$^+$ GL neurons derive predominantly from anterior/medial, carousal/dorsal, and ventral subpopulations of NSCs, respectively (Merkle et al., 2007, 2014). However, experimental data reported in these studies indicate that the correlation between these neuronal subtypes and the topological locations of NSCs is not a strict match but reflects an overall trend only. In fact, the current study, together with our previous report (López-Juárez et al., 2013), demonstrates that both Olig2$^+$ and Gsx2$^+$ NSCs generate CR$^+$ neurons in the GL despite the fact that they are mutually exclusive stem cell pools in the postnatal SVZ. Moreover, although Olig2$^+$ NSCs are abundant in the vSVZ, our fate-mapping study did not detect the generation of CB$^+$ GL neurons by these ventral Olig2$^+$ NSCs. Thus, not all NSCs in the vSVZ are responsible for the generation of CB$^+$ neurons. As such, the notion that particular subtypes of OB neurons marked by existing markers are generated solely by a specific group of NSCs that exist in particular SVZ subdomains only is not supported by available data and certainly an oversimplification. Rather, our study and existing data support the idea that neurons expressing the same known molecular markers are likely to be produced by heterogeneous NSC populations that may exist in multiple SVZ subdomains.

Developmental changes in the molecular properties of Olig2-expressing NSCs/progenitors

Similarities and differences between NSCs/progenitors in the developing and adult brain have been extensively studied (Fuentealba et al., 2015; Götz et al., 2016). However, a difficulty in such comparisons is that NSCs/progenitors are highly heterogeneous in different regions of the embryonic and postnatal brains, and such heterogeneity changes over time. scRNA-seq analysis of Olig2$^+$ NSCs/progenitors at different stages provides us with a unique opportunity to compare equivalent NSC populations at distinct stages at the molecular level. We found that, although Olig2$^+$ NSCs/progenitors at each developmental stage intrinsically comprise heterogeneous cell populations, cells belonging to each stage as a whole form a unique cell cluster compared with cells at other developmental stages (Fig. 5). Our analysis further revealed that changes in cell cycle and metabolic/signaling pathways contribute significantly to such stepwise developmental transitions. For example, the fraction of cells in the G0/G1 phase markedly increased from 7% to 35% between E12.5 and E18.5 and was further elevated at the P14 (41%) and adult (72%) stages. Such stepwise increases in cells in the G0/G1 phase were accompanied by gradual decreases of cells in both the S and G2/M phases. Molecular pathway analysis also revealed that the activity of the signaling pathways for NTF receptors was initially low at E12.5 but gradually increased from E18.5 to the adult stage, whereas a group of lipid metabolism and neurotransmission/ion transport-related pathways did not become active until NSCs reached the adult stage. Further investigations of these scRNA-seq datasets will help us to better understand the molecular mechanisms underlying the developmental transitions of NSCs/progenitors from early embryonic to adult stages.

MATERIALS AND METHODS

Animals

All animal procedures were performed according to the guidelines of the National Institute of Health and the Institutional Animal Care and Use Committee. Embryos were collected at E12.5, E15.5 and E18.5 (the day on which the copulatory plug was found was considered to be E0.5). Brains of P14 and P16 pups and adult animals from both females and males at the age of 10-12 weeks were collected after cardiac perfusion with 4% (v/v) paraformaldehyde (PFA) in PBS. Details of the mouse lines and their handling are described in the supplementary Materials and Methods.

Histology

Cryosections (12 µm) of embryos and vibratome sections (30 µm) of postnatal and adult brains were used for immunostaining. The method used to identify specific subdomains of the SVZ and the antibodies used for immunostaining are described in the supplementary Materials and Methods. Fluorescent images were captured using a Nikon A1R si laser scanning confocal microscope. Quantitative results are expressed as the mean±standard deviation (s.d.) of data obtained from three to four animals for each genotype. All statistical analyses were performed using R software (version R 3.5.0: https://www.r-project.org/) (for details, see the supplementary Materials and Methods).

scRNA-seq

scRNA-seq data on E12.5 ventral telencephalon have been described previously (GSE42768: Roychoudhury et al., 2020), and the other three datasets on E18.5, P14 and adult cells generated in this study are available from GEO under the accession number GSE174392. Details of the generation and analysis of scRNA-seq data are described in the supplementary Materials and Methods.

Acknowledgements

We are grateful to Magdalena Götz, Jane Johnson, Hirohide Takebayashi and Kazuaki Yoshikawa for reagents, and to Matthew Kofron, Evan Meyer, Sarah McLeod, Diane Girard, Jordan Burge and Amber Niederhelman for technical support.

Competing interests

The authors declare no competing or financial interests.

Author contributions

Conceptualization: Á.d.Á., M.A., M.N.; Methodology: Á.d.Á., M.A., S.S.P., M.N.; Software: M.A., N.S., S.S.P.; Validation: M.N.; Formal analysis: Á.d.Á., M.A., N.S., S.S.P., M.N.; Investigation: Á.d.Á., M.A., M.N.; Resources: K.U., S.Q., J.E., D.N., J.S., B.G., Q.R.L., S.S.P., R.W., K.C., M.N.; Data curation: Á.d.Á., M.A., K.U., N.S., S.Q., J.E., D.N., J.S., S.S.P., R.W., K.C., M.N.; Writing - original draft: Á.d.Á., M.N.; Writing - review & editing: Á.d.Á., M.A., N.S., S.Q., J.E., D.N., J.S., B.G., Q.R.L., S.S.P., R.W., K.C., M.N.; Visualization: M.A., M.N.; Supervision: M.N.; Project administration: M.N.; Funding acquisition: M.N.

Funding

This study was supported by the National Institutes of Health (2R01NS069893 to M.N. and K.C.), by the Ohio Eminent Scholar Fund from the State of Ohio to M.N. and by a Chan Zuckerberg Initiative grant (2017-173968) to S.S.P. Deposited in PMC for release after 12 months.

Data availability

scRNA-seq data on E18.5, P14 and adult cells generated in this study are available from GEO under the accession number GSE174392.

Peer review history

The peer review history is available online at https://journals.biologists.com/dev/article-lookup/doi/10.1242/dev.200028.

References

Andersen, J., Urbán, N., Achimastou, A., Ito, A., Simic, M., Ullom, K., Martynoga, B., Lebel, M., Göritz, C., Frisén, J. et al. (2014). A transcriptional mechanism integrating inputs from extracellular signals to activate hippocampal stem cells. *Neuron* **83**, 1085-1097. doi:10.1016/j.neuron.2014.08.004

Batista-Brito, R., Close, J., Machold, R. and Fishell, G. (2008). The distinct temporal origins of olfactory bulb interneuron subtypes. *J. Neurosci.* **28**, 3966-3975. doi:10.1523/JNEUROSCI.5625-07.2008

Becht, E., McInnes, L., Healy, J., Dutertre, C.-A., Kwok, I. W. H., Ng, L. G., Ginhoux, F. and Newell, E. W. (2018). Dimensionality reduction for visualizing single-cell data using UMAP. *Nat. Biotechnol.* **37**, 38-44. doi:10.1038/nbt.4314

Brill, M. S., Snapyan, M., Wohlfrom, H., Ninkovic, J., Jawerka, M., Mastick, G. S., Ashery-Padan, R., Saghatelyan, A., Berninger, B. and Götz, M. (2008). A dlx2- and pax6-dependent transcriptional code for periglomerular neuron specification in the adult olfactory bulb. *J. Neurosci.* **28**, 6439-6452. doi:10.1523/JNEUROSCI.0700-08.2008

Briñón, J. G., Martinez-Guijarro, F. J., Bravo, I. G., Arevalo, R., Crespo, C., Okazaki, K., Hidaka, H., Aijon, J. and Alonso, J. R. (1999). Coexpression of neurocalcin with other calcium-binding proteins in the rat main olfactory bulb. *J. Comp. Neurol.* **407**, 404-414. doi:10.1002/(SICI)1096-9861(19990510)407:3<404::AID-CNE8>3.0.CO;2-9

Cai, J., Chen, Y., Cai, W.-H., Hurlock, E. C., Wu, H., Kernie, S. G., Parada, L. F. and Lu, Q. R. (2007). A crucial role for Olig2 in white matter astrocyte development. *Development* **134**, 1887-1899. doi:10.1242/dev.02847

Casarosa, S., Fode, C. and Guillemot, F. (1999). Mash1 regulates neurogenesis in the ventral telencephalon. *Development* **126**, 525-534. doi:10.1242/dev.126.3.525

Cebrian-Silla, A., Nascimento, M. A., Redmond, S. A., Mansky, B., Wu, D., Obernier, K., Rodriguez, R. R., Gonzalez-Granero, S., García-Verdugo, J. M., Lim, D. A. et al. (2021). Single-cell analysis of the ventricular-subventricular zone reveals signatures of dorsal and ventral adult neurogenesis. *eLife* **10**, e67436. doi:10.7554/eLife.67436.sa2

Chapman, H., Waclaw, R. R., Pei, Z., Nakafuku, M. and Campbell, K. (2013). The homeobox gene Gsx2 controls the timing of oligodendroglial fate specification in mouse lateral ganglionic eminence progenitors. *Development* **140**, 2289-2298. doi:10.1242/dev.091090

Chapman, H., Riesenberg, A., Ehrman, L. A., Kohli, V., Nardini, D., Nakafuku, M., Campbell, K. and Waclaw, R. R. (2018). Gsx transcription factors control neuronal versus glial specification in ventricular zone progenitors of the mouse lateral ganglionic eminence. *Dev. Biol.* **442**, 115-126. doi:10.1016/j.ydbio.2018.07.005

Coré, N., Erni, A., Hoffmann, H. M., Mellon, P. L., Saurin, A. J., Beclin, C. and Cremer, H. (2020). Stem cell regionalization during olfactory bulb neurogenesis depends on regulatory interactions between *Vax1* and *Pax6*. *eLife* **9**, e58215. doi:10.7554/eLife.58215

de Chevigny, A., Coré, N., Follert, P., Gaudin, M., Barbry, P., Béclin, C. and Cremer, H. (2012). miR-7a regulation of Pax6 controls spatial origin of forebrain dopaminergic neurons. *Nat. Neurosci.* **15**, 1120-1126. doi:10.1038/nn.3142

Delgado, R. N. and Lim, D. A. (2015). Embryonic Nkx2.1-expressing neural precursor cells contribute to the regional heterogeneity of adult V-SVZ neural stem cells. *Dev. Biol.* **407**, 265-274. doi:10.1016/j.ydbio.2015.09.008

Dessaud, E., Yang, L. L., Hill, K., Cox, B., Ulloa, F., Ribeiro, A., Mynett, A., Novitch, B. G. and Briscoe, J. (2007). Interpretation of the sonic hedgehog morphogen gradient by a temporal adaptation mechanism. *Nature* **450**, 717-720. doi:10.1038/nature06347

Doetsch, F., Petreanu, L., Caille, I., Garcia-Verdugo, J.-M. and Alvarez-Buylla, A. (2002). EGF converts transit-amplifying neurogenic precursors in the adult brain into multipotent stem cells. *Neuron* **36**, 1021-1034. doi:10.1016/S0896-6273(02)01133-9

Dulken, B. W., Leeman, D. S., Boutet, S. C., Hebestreit, K. and Brunet, A. (2017). Single-cell transcriptomic analysis defines heterogeneity and transcriptional dynamics in the adult neural stem cell lineage. *Cell Rep.* **18**, 777-790. doi:10.1016/j.celrep.2016.12.060

Emery, B. and Lu, Q. R. (2015). Transcriptional and epigenetic regulation of oligodendrocyte development and myelination in the central nervous system. *Cold Spring Harb. Perspect. Biol.* **7**, a020461. doi:10.1101/cshperspect.a020461

Fish, J. L., Dehay, C., Kennedy, H. and Huttner, W. B. (2008). Making bigger brains-the evolution of neural-progenitor-cell division. *J. Cell Sci.* **121**, 2783-2793. doi:10.1242/jcs.023465

Fuentealba, L. C., Rompani, S. B., Parraguez, J. I., Obernier, K., Romero, R., Cepko, C. L. and Alvarez-Buylla, A. (2015). Embryonic origin of postnatal neural stem cells. *Cell* **161**, 1644-1655. doi:10.1016/j.cell.2015.05.041

Götz, M., Nakafuku, M. and Petrik, D. (2016). Neurogenesis in the developing and adult brain-similarities and key differences. *Cold Spring Harb. Perspect. Biol.* **8**, a018853. doi:10.1101/cshperspect.a018853

Griss, J., Viteri, G., Sidiropoulos, K., Nguyen, V., Fabregat, A. and Hermjakob, H. (2020). ReactomeGSA - efficient multi-omics comparative pathway analysis. *Mol. Cell. Proteomics* **19**, 2115-2125. doi:10.1074/mcp.TIR120.002155

Hack, M. A., Saghatelyan, A., de Chevigny, A., Pfeifer, A., Ashery-Padan, R., Lledo, P.-M. and Götz, M. (2005). Neuronal fate determinants of adult olfactory bulb neurogenesis. *Nat. Neurosci.* **8**, 865-872. doi:10.1038/nn1479

Hänzelmann, S., Castelo, R. and Guinney, J. (2013). GSVA: gene set variation analysis for microarray and RNA-seq data. *BMC Bioinformatics* **14**, 7. doi:10.1186/1471-2105-14-7

Haubensak, W., Attardo, A., Denk, W. and Huttner, W. B. (2004). Neurons arise in the basal neuroepithelium of the early mammalian telencephalon: a major site of neurogenesis. *Proc. Natl. Acad. Sci. USA* **101**, 3196-3201. doi:10.1073/pnas.0308600100

Kohwi, M., Osumi, N., Rubenstein, J. L. R. and Alvarez-Buylla, A. (2005). Pax6 is required for making specific subpopulations of granule and periglomerular neurons in the olfactory bulb. *J. Neurosci.* **25**, 6997-7003. doi:10.1523/JNEUROSCI.1435-05.2005

Kohwi, M., Petryniak, M. A., Long, J. E., Ekker, M., Obata, K., Yanagawa, Y., Rubenstein, J. L. R. and Alvarez-Buylla, A. (2007). A subpopulation of olfactory bulb GABAergic interneurons is derived from Emx1- and Dlx5/6-expressing progenitors. *J. Neurosci.* **27**, 6878-6891. doi:10.1523/JNEUROSCI.0254-07.2007

Lemasson, M., Saghatelyan, A., Olivo-Marin, J.-C. and Lledo, P.-M. (2005). Neonatal and adult neurogenesis provide two distinct populations of newborn neurons to the mouse olfactory bulb. *J. Neurosci.* **25**, 6816-6825. doi:10.1523/JNEUROSCI.1114-05.2005

Lledo, P.-M. and Valley, M. (2016). Adult olfactory bulb neurogenesis. *Cold Spring Harb. Perspect. Biol.* **8**, a018945. doi:10.1101/cshperspect.a018945
Long, J. E., Garel, S., Alvarez-Dolado, M., Yoshikawa, K., Osumi, N., Alvarez-Buylla, A. and Rubenstein, J. L. R. (2007). Dlx-dependent and -independent regulation of olfactory bulb interneuron differentiation. *J. Neurosci.* **27**, 3230-3243. doi:10.1523/JNEUROSCI.5265-06.2007
López-Juárez, A., Howard, J., Ullom, K., Howard, L., Grande, A., Pardo, A., Waclaw, R., Sun, Y.-Y., Yang, D., Kuan, C.-Y. et al. (2013). Gsx2 controls region-specific activation of neural stem cells and injury-induced neurogenesis in the adult subventricular zone. *Genes Dev.* **27**, 1272-1287. doi:10.1101/gad.217539.113
Lyons, G. E., Micales, B. K., Schwarz, J., Martin, J. F. and Olson, E. N. (1995). Expression of mef2 genes in the mouse central nervous system suggests a role in neuronal maturation. *J. Neurosci.* **15**, 5727-5738. doi:10.1523/JNEUROSCI.15-08-05727.1995
Madisen, L., Zwingman, T. A., Sunkin, S. M., Oh, S. W., Zariwala, H. A., Gu, H., Ng, L. L., Palmiter, R. D., Hawrylycz, M. J., Jones, A. R. et al. (2010). A robust and high-throughput Cre reporting and characterization system for the whole mouse brain. *Nat. Neurosci.* **13**, 133-140. doi:10.1038/nn.2467
Menn, B., Garcia-Verdugo, J. M., Yaschine, C., Gonzalez-Perez, O., Rowitch, D. and Alvarez-Buylla, A. (2006). Origin of oligodendrocytes in the subventricular zone of the adult brain. *J. Neurosci.* **26**, 7907-7918. doi:10.1523/JNEUROSCI.1299-06.2006
Merkle, F. T., Mirzadeh, Z. and Alvarez-Buylla, A. (2007). Mosaic organization of neural stem cells in the adult brain. *Science* **317**, 381-384. doi:10.1126/science.1144914
Merkle, F. T., Fuentealba, L. C., Sanders, T. A., Magno, L., Kessaris, N. and Alvarez-Buylla, A. (2014). Adult neural stem cells in distinct microdomains generate previously unknown interneuron types. *Nat. Neurosci.* **17**, 207-214. doi:10.1038/nn.3610
Miyoshi, G., Butt, S. J. B., Takebayashi, H. and Fishell, G. (2007). Physiologically distinct temporal cohorts of cortical interneurons arise from telencephalic Olig2-expressing precursors. *J. Neurosci.* **27**, 7786-7798. doi:10.1523/JNEUROSCI.1807-07.2007
Mizrak, D., Levitin, H. M., Delgado, A. C., Crotet, V., Yuan, J., Chaker, Z., Silva-Vargas, V., Sims, P. A. and Doetsch, F. (2019). Single-cell analysis of regional differences in adult v-svz neural stem cell lineages. *Cell Rep.* **26**, 394-406.e5. doi:10.1016/j.celrep.2018.12.044
Mori, T., Tanaka, K., Buffo, A., Wurst, W., Kühn, R. and Götz, M. (2006). Inducible gene deletion in astroglia and radial glia–a valuable tool for functional and lineage analysis. *Glia* **54**, 21-34. doi:10.1002/glia.20350
Nakafuku, M. and del Águila, Á. (2020). Developmental dynamics of neurogenesis and gliogenesis in the postnatal mammalian brain in health and disease: Historical and future perspectives. *Wiley Interdiscip. Rev. Dev. Biol.* **9**, e369. doi:10.1002/wdev.369
Nakafuku, M. and Grande, A. W. (2020). Neurogenesis in the damaged mammalian brain. In *Patterning and cell type specification in the developing CNS and PNS*, 2nd edn. (ed. J. L. R. Rubenstein and P. Rakic), pp. 523–597. Academic Press.
Noctor, S. C., Martínez-Cerdeño, V., Ivic, L. and Kriegstein, A. R. (2004). Cortical neurons arise in symmetric and asymmetric division zones and migrate through specific phases. *Nat. Neurosci.* **7**, 136-144. doi:10.1038/nn1172
Ono, K., Takebayashi, H., Ikeda, K., Furusho, M., Nishizawa, T., Watanabe, K. and Ikenaka, K. (2008). Regional- and temporal-dependent changes in the differentiation of Olig2 progenitors in the forebrain, and the impact on astrocyte development in the dorsal pallium. *Dev. Biol.* **320**, 456-468. doi:10.1016/j.ydbio.2008.06.001
Ortega, F., Gascón, S., Masserdotti, G., Deshpande, A., Simon, C., Fischer, J., Dimou, L., Chichung Lie, D., Schroeder, T. and Berninger, B. (2013). Oligodendrogliogenic and neurogenic adult subependymal zone neural stem cells constitute distinct lineages and exhibit differential responsiveness to Wnt signalling. *Nat. Cell Biol.* **15**, 602-613. doi:10.1038/ncb2736
Parrish-Aungst, S., Shipley, M. T., Erdelyi, F., Szabo, G. and Puche, A. C. (2007). Quantitative analysis of neuronal diversity in the mouse olfactory bulb. *J. Comp. Neurol.* **501**, 825-836. doi:10.1002/cne.21205
Pastrana, E., Cheng, L.-C. and Doetsch, F. (2009). Simultaneous prospective purification of adult subventricular zone neural stem cells and their progeny. *Proc. Natl. Acad. Sci. USA* **106**, 6387-6392. doi:10.1073/pnas.0810407106
Paul, A., Chaker, Z. and Doetsch, F. (2017). Hypothalamic regulation of regionally distinct adult neural stem cells and neurogenesis. *Science* **356**, 1383-1386. doi:10.1126/science.aal3839
Petryniak, M. A., Potter, G. B., Rowitch, D. H. and Rubenstein, J. L. R. (2007). Dlx1 and Dlx2 control neuronal versus oligodendroglial cell fate acquisition in the developing forebrain. *Neuron* **55**, 417-433. doi:10.1016/j.neuron.2007.06.036
Qin, S., Ware, S. M., Waclaw, R. R. and Campbell, K. (2017). Septal contributions to olfactory bulb interneuron diversity in the embryonic mouse telencephalon: role of the homeobox gene Gsx2. *Neural Dev.* **12**, 13. doi:10.1186/s13064-017-0090-5
Roychoudhury, K., Salomone, J., Qin, S., Cain, B., Adam, M., Potter, S. S., Nakafuku, M., Gebelein, B. and Campbell, K. (2020). Physical interactions between Gsx2 and Ascl1 balance progenitor expansion versus neurogenesis in the mouse lateral ganglionic eminence. Development **147**, dev185348. doi:10.1242/dev.185348
Sakamoto, M., Ieki, N., Miyoshi, G., Mochimaru, D., Miyachi, H., Imura, T., Yamaguchi, M., Fishell, G., Mori, K., Kageyama, R. et al. (2014). Continuous postnatal neurogenesis contributes to formation of the olfactory bulb neural circuits and flexible olfactory associative learning. *J. Neurosci.* **34**, 5788-5799. doi:10.1523/JNEUROSCI.0674-14.2014
Shibata, M., Nakao, H., Kiyonari, H., Abe, T. and Aizawa, S. (2011). MicroRNA-9 regulates neurogenesis in mouse telencephalon by targeting multiple transcription factors. *J. Neurosci.* **31**, 3407-3422. doi:10.1523/JNEUROSCI.5085-10.2011
Stenman, J., Toresson, H. and Campbell, K. (2003). Identification of two distinct progenitor populations in the lateral ganglionic eminence: implications for striatal and olfactory bulb neurogenesis. *J. Neurosci.* **23**, 167-174. doi:10.1523/JNEUROSCI.23-01-00167.2003
Takebayashi, H., Nabeshima, Y., Yoshida, S., Chisaka, O., Ikenaka, K. and Nabeshima, Y.-I. (2002). The basic helix-loop-helix factor olig2 is essential for the development of motoneuron and oligodendrocyte lineages. *Curr. Biol.* **12**, 1157-1163. doi:10.1016/S0960-9822(02)00926-0
Toresson, H. and Campbell, K. (2001). A role for Gsh1 in the developing striatum and olfactory bulb of Gsh2 mutant mice. *Development* **128**, 4769-4780. doi:10.1242/dev.128.23.4769
Toresson, H., Potter, S. S. and Campbell, K. (2000). Genetic control of dorsal-ventral identity in the telencephalon: opposing roles for Pax6 and Gsh2. *Development* **127**, 4361-4371. doi:10.1242/dev.127.20.4361
Torii, M., Matsuzaki, F., Osumi, N., Kaibuchi, K., Nakamura, S., Casarosa, S., Guillemot, F. and Nakafuku, M. (1999). Transcription factors Mash-1 and Prox-1 delineate early steps in differentiation of neural stem cells in the developing central nervous system. *Development* **126**, 443-456. doi:10.1242/dev.126.3.443
Waclaw, R. R., Wang, B., Pei, Z., Ehrman, L. A. and Campbell, K. (2009). Distinct temporal requirements for the homeobox gene Gsx2 in specifying striatal and olfactory bulb neuronal fates. *Neuron* **63**, 451-465. doi:10.1016/j.neuron.2009.07.015
Wang, B., Waclaw, R. R., Allen, Z. J., II, Guillemot, F. and Campbell, K. (2009). Ascl1 is a required downstream effector of Gsx gene function in the embryonic mouse telencephalon. *Neural Dev.* **4**, 5. doi:10.1186/1749-8104-4-5
Wang, B., Long, J. E., Flandin, P., Pla, R., Waclaw, R. R., Campbell, K. and Rubenstein, J. L. R. (2013). Loss of Gsx1 and Gsx2 function rescues distinct phenotypes in Dlx1/2 mutants. *Comp. Neurol.* **521**, 1561-1584. doi:10.1002/cne.23242
Wang, H., Xu, L., Lai, C., Hou, K., Chen, J., Guo, Y., Sambangi, A., Swaminathan, S., Xie, C., Wu, Z. et al. (2021). Region-specific distribution of Olig2-expressing astrocytes in adult mouse brain and spinal cord. *Mol. Brain* **14**, 36. doi:10.1186/s13041-021-00747-0
Wilsch-Bräuninger, M., Florio, M. and Huttner, W. B. (2016). Neocortex expansion in development and evolution - from cell biology to single genes. *Curr. Opin. Neurobiol.* **39**, 122-132. doi:10.1016/j.conb.2016.05.004
Xie, X. P., Laks, D. R., Sun, D., Poran, A., Laughney, A. M., Wang, Z., Sam, J., Belenguer, G., Fariñas, I., Elemento, O. et al. (2020). High-resolution mouse subventricular zone stem-cell niche transcriptome reveals features of lineage, anatomy, and aging. *Proc. Natl. Acad. Sci. USA* **117**, 31448-31458. doi:10.1073/pnas.2014389117
Young, K. M., Fogarty, M., Kessaris, N. and Richardson, W. D. (2007). Subventricular zone stem cells are heterogeneous with respect to their embryonic origins and neurogenic fates in the adult olfactory bulb. *J. Neurosci.* **27**, 8286-8296. doi:10.1523/JNEUROSCI.0476-07.2007
Yue, T., Xian, K., Hurlock, E., Xin, M., Kernie, S. G., Parada, L. F. and Lu, Q. R. (2006). A critical role for dorsal progenitors in cortical myelination. *J. Neurosci.* **26**, 1275-1280. doi:10.1523/JNEUROSCI.4717-05.2006
Yun, K., Potter, S. and Rubenstein, J. L. (2001). Gsh2 and Pax6 play complementary roles in dorsoventral patterning of the mammalian telencephalon. *Development* **128**, 193-205. doi:10.1242/dev.128.2.193
Yun, K., Fischman, S., Johnson, J., de Angelis, M. H., Weinmaster, G. and Rubenstein, J. L. R. (2002). Modulation of the notch signaling by Mash1 and Dlx1/2 regulates sequential specification and differentiation of progenitor cell types in the subcortical telencephalon. *Development* **129**, 5029-5040. doi:10.1242/dev.129.21.5029
Yun, K., Garel, S., Fischman, S. and Rubenstein, J. L. R. (2003). Patterning of the lateral ganglionic eminence by the Gsh1 and Gsh2 homeobox genes regulates striatal and olfactory bulb histogenesis and the growth of axons through the basal ganglia. *J. Comp. Neurol.* **461**, 151-165. doi:10.1002/cne.10685
Yuzwa, S. A., Borrett, M. J., Innes, B. T., Voronova, A., Ketela, T., Kaplan, D. R., Bader, G. B. and Miller, F. D. (2017). Developmental emergence of adult neural stem cells as revealed by single-cell transcriptional profiling. *Cell Rep.* **21**, 3970-3986. doi:10.1016/j.celrep.2017.12.017
Zywitza, V., Misios, A., Bunatyan, L., Willnow, T. E. and Rajewsky, N. (2018). Single-cell transcriptomics characterizes cell types in the subventricular zone and uncovers molecular defects impairing adult neurogenesis. *Cell Rep.* **25**, 2457-2469.e8. doi:10.1016/j.celrep.2018.11.003

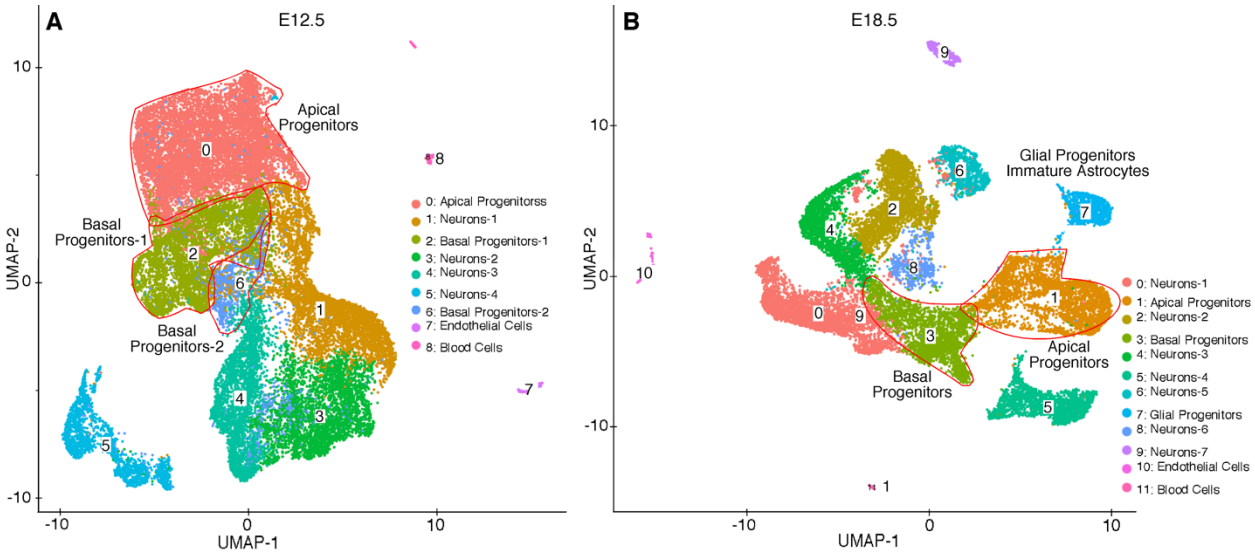

Fig. S1. scRNA-seq analysis of cells in the ventral telencephalon at E12.5 and E18.5. UMAP plots of distinct cell types in the whole ventral telencephalon at E12.5 (A) and E18.5 (B). Nine and twelve molecularly distinct cell types are identified among cells E12.5 and E18.5, respectively, and are shown in different colors and numbers. The cell type of each cell cluster was identified based on the profile of genes with enriched expression in each cluster. Clusters with characteristics of NSC/progenitors (clusters 0, 2, and 6 in A and clusters 1 and 3 in B) are outlined and labeled in red.

Table S1. Genes enriched in distinct cell clusters at different stages.

Click here to download Table S1

Table S2. Genes enriched in Olig2^{+} NSCs/progenitors at different stages.

Click here to download Table S2

Table S3. Genes enriched in distinct cell clusters among Olig2^{+} NSCs/progenitors at all stages.

Click here to download Table S3

Table S4. List of cell cycle phase-selective genes.

Click here to download Table S4

Table S5. Pathway analysis among Olig2^{+} NSCs/progenitors at all stages.

Click here to download Table S5

Supplementary Materials and Methods

***Mouse Lines*:** The generation and genotyping of mice carrying *Olig2*^{flox} (Yue et al., 2006; Cai et al., 2007), *Gsx2*^{flox} (Waclaw et al., 2009), *Olig2*^{CreER} (Takebayashi et al., 2002), *GLAST*^{CreER} (Mori et al., 2006), and *Rosa-tdTomato (Ai14)* [Jackson Laboratory Stock number 007914, ref. Madisen et al., 2010] are described in previous studies. For conditional inactivation of *Olig2*, two sets of animals were generated and examined. First, for conditional inactivation of *Olig2* in GLAST^{+} adult NSCs, *Olig2*$^{flox/+}$*;GLAST*$^{CreER/+}$ and *Olig2*$^{flox/+}$*;Rosa-tdTomato*$^{+/- \text{ or } +/+}$ mice were crossed to obtain *Olig2*$^{flox/flox}$*;GLAST*$^{CreER/+}$*;Rosa-tdTomato*$^{+/- \text{ or } +/+}$ (*Olig2 cKO*) mice. Littermates carrying *Olig2*$^{flox/+}$ and *Olig2*$^{+/+}$ alleles were used as control. Second, for lineage tracing of progeny of Olig2-expressing NSCs after *Olig2* inactivation, *Olig2*$^{CreER/+}$*;Rosa-tdTomato*$^{+/-}$ and *Olig2*$^{flox/+}$*;Rosa-tdTomato*$^{+/-}$ mice were crossed to generate *Olig2*$^{CreER/flox}$*;Rosa-tdTomato*$^{+/- \text{ or } +/+}$ (*Olig2-CreER cKO*) mice, in which Olig2 is inactivated and tdTomato is expressed selectively in prospective Olig2-expressing NSCs. *Olig2*$^{CreER/+}$*;Rosa-tdTomato*$^{+/- \text{ or } +/+}$ (*Olig2-CreER*) littermates were used as control. For analysis of *Olig2* and *Gsx2* mutant embryos, *Olig2*$^{cre/+}$ (Dessaud et al., 2007) and *Gsx2*$^{RA/+}$ mice ("RA" refers to the germline "recombined allele" from the *Gsx2*^{flox} allele; Wang et al., 2009) carrying the null alleles of *Olig2* and *Gsx2*, respectively, were crossed to generate *Olig2* and *Gsx2* mutant embryos at E15.5.

***Animal Handling*:** Administration of Tx and BrdU to animals was performed at the time when mice reached the age of 10-12 weeks. To induce CreER-dependent recombination, mice received intraperitoneal (ip) injections of Tx (100 mg/kg of body weight, 20 mg/ml in corn oil) once daily for either 2 or 10 days (treatments for 5 consecutive days, followed by 2 days of resting and another round of treatments for 5 days) for D3 and D56 animals, respectively. To fate-map progeny of

proliferative cells in vivo, animals received BrdU by ip injection (50 mg/kg body weight) twice per day (6 hours apart) for 5 days and were subsequently kept alive without BrdU for additional 3 weeks before sacrifice. Previous studies have shown that it takes 3-6 weeks for newly generated neurons in the SVZ to reach the OB and express mature markers (For example, see Kohwi et al., 2007, Sakamoto et al., 2014, and references therein). Thus, to allow for many tdTomato$^+$ cells derived from Olig2$^+$ NSCs to settle in their final destinations within the OB and express specific markers, we chose D56 after the first Tx injection followed by a 3-week chase period after BrdU injections as the point of analysis.

***Histology*:** For quantitative analysis of immunopositive cells, 12 μm-thick cryosections for the adult OB and embryonic brains and 30 μm-thick vibratome sections for the P14 and adult brains were examined. For the latter, sections that covered the following coronal planes were selected according to a mouse brain atlas (Paxinos and Franklin, 2008) (positions are relative to the bregma): OB, +3.9 to +4.0 mm; RMS, +2.0 to +2.1 mm; anterior SVZ, + 1.4 to +1.5 mm; typical SVZ, +0.7 to +1.0 mm; posterior SVZ, -0.3 to -0.5 mm; and hippocampal SVZ, -1.6 to -1.8 mm. Six subregions of the SVZ along the DV and mediolateral axes are defined as follows: dorsal roof (callosal) SVZ, the area between the ependymal layer and the overlaying corpus callosum encompassing the dorsal roof of the LV; dlSVZ, the high cell-density area adjacent to the dorsal one-third of the lateral wall of the LV medially and the corpus callosum dorsally; lSVZ, the areas adjacent to the middle one-third of the lateral wall of the LV; mSVZ, the areas adjacent to the middle one-third of the medial wall of the LV; and vSVZ, the high cell-density area adjacent to the ventral one-third of the LV.

Immunoreactive cells were visualized by staining with secondary antibodies conjugated

with Alexa Fluor 488, 568, and 647. Cell nuclei were stained with 4',6-diamidino-2-phenylindole (DAPI). Fluorescent images were captured using Nikon A1R si laser scanning confocal microscope. A series of 62 z-plane images of vibratome sections with an optical resolution of 0.325 fÊm and 5 z-plane images of cryosections with an optical resolution of 0.80 fÊm were obtained using a 40x lens and subsequently analyzed using Fiji (Rasband, W.S., ImageJ, U. S. National Institutes of Health, Bethesda, Maryland, USA, https://imagej.nih.gov/ij/, 1997-2018). Immunoreactivity of individual cells for particular antigens was assessed by evaluating serial z plane images that encompassed the cell body of each cell after setting an appropriate threshold of signal strength for each antigen. The nuclei of individual cells were first identified with an aid of DAPI signals. As for immunoreactivity of transcription factors such as Olig2 and Dlx2, clear overlaps between nuclear immunoreactive signals and DAPI signals were judged as positive. Regarding cytoplasmic and cytoskeletal antigens such as Dcx and GFAP, cells that clearly showed diffuse and/or fibrous immunoreactive signals that surrounded their DAPI+ nuclei were considered to be immunepositive. Immunostaining was performed as described previously (Lopez-Juarez et al., 2013; Andersen et al., 2014) using antibodies listed below:

Antigen	**Species**	**Source**	**Catalog #**	**Condition**	**Reference**
Olig2	Rabbit	Millipore-Sigma	AB9610	1:500	Toresson et al., 2000
Olig2	Goat	R&D Systems	AF2418	1:4000	-
Olig1	Rabbit	Millipore-Sigma	AB15620	1:2000	
Gsx2	Rabbit	In-house	-	1:2000	Toresson et al., 2000
Gsx1	Guinea Pig	In-house	-	1:4000	Chapman et al., 2018
Nkx2.1	Rabbit	Seven Hills Bioreagents	WRAB-123	1:1000	-
Pax6	Rabbit	Biolegend	901301	1:500	-
GFAP	Mouse	Sigma-Aldrich	G-3893	1:2000	-

Ascl1	Guinea Pig	Jane Johnson	-	1:40000	Battiste et al., 2007
“	Rabbit	Abcam	AB74065	1:4000	
Ki67	Rabbit	Novocastra	NLC-Ki67P	1:1000	-
Dlx2	Guinea Pig	Kazuaki Yoshikawa	-	1:2000	Kuwajima et al., 2006
NeuN	Rabbit	Cell Signaling		1:5000	
Dcx	Chicken	Abcam	ab153668	1:1000	-
CR	Goat	SWANT	CG1	1:3000	-
NC	Rabbit	ProteinTech Group	12925-1-AP	1:1000	-
TH	Rabbit	Millipore	AB152	1:500	-
CB	Mouse	Sigma-Aldrich	C8666	1:5000	-
PV	Guinea Pig	Millipore	AB15738	1:5000	-
Mef2c	Rabbit	ProteinTech Group	10056-1-AP	1:2000	-
BrdU	Rat	Oxford Biotech	OBT0030	1:200	-

Statistical analysis: The quantitative results of histological analysis are expressed as means $\pm$ standard deviation (S.D.) of data obtained from 3 to 5 animals for each genotype. Normality and homoscedasticity of the data were evaluated by Shapiro-Wilk and Bartlett's tests, respectively. Statistical differences between genotypes were evaluated by Student’s t-test for parametric data and Welch’s t-test for non-parametric data. All these statistical analyses were performed using R software (version R 3.6.3 GUI 1.70: https://www.r-project.org/).

scRNA-seq analysis: For single-cell transcriptome analysis of NSCs/progenitors, two independent sets of samples were prepared and examined for each stage. For embryonic samples, the whole ventral telencephalon (including the LGE, MGE, POA, and septum) was dissected out from wild type CD1 embryos at E12.5 and E18.5 under microscope and subsequently dissociated into single

cells using Ca^{2+}/Mg^{2+}-free Dulbecco's PBS containing 0.05% (w/v) trypsin and 0.02% (w/v) sodium ethylenediaminetetraacetic acid (EDTA-Na) as described previously (Roychoudhury et al., 2020). For postnatal SVZ samples, 1 mm-thick coronal slices of brains were prepared from P14 and adult (10- to 12-week old) wild type mice using a brain slicer, and thin SVZ tissue strips around the LV were dissected out under microscope. The isolated tissues were dissociated into single cells using Ca^{2+}/Mg^{2+}-free Hanks' balanced salt solution (HBSS) containing collagenase type VI (10 units/ml) and dispase II (2 units/ml) as described previously (Nagao et al., 2008). The single cell suspension of each sample was adjusted to 1000 cells/μl and approximately 12,000 cells were loaded into a well on a 10x Chromium Single Cell instrument (10x Genomics). Barcoding, cDNA amplification and library construction were performed using the Chromium Single Cell 3' Reagent Kits v3 according to the manufacturer's instructions. Post cDNA amplification reaction and cleanup were performed using SPRI select reagent (Beckman Coulter, Cat# B23318). Post cDNA amplification and library construction quality were analyzed using the Agilent Bioanalyzer High Sensitivity kit (Agilent 5067–4626). The final single cell 3' library contains standard Illumina paired-end constructs (begin and end with P5 and P7 primer sequences, and 16 bp 10x Barcode, 10 bp UMI, Read one primer sequence, Read two primer sequence, and the 8 bp i7 sample index). Libraries were sequenced using an Illumina HiSeq 2500 and the paired-end 75 bp sequencing flow cell. Sequencing parameters used were: Read 1, 27 cycles; i7 index, eight cycles; Read 2, 147 cycles, according to manufacturer's recommendations, which produced about 300 million reads.

Initial analysis of the duplicated data sets from each stage (E12.5, E18.5, P14, and adult) produced very similar results so that they were merged as a single dataset, and potential doublets were removed using DoubletDecon (DePasquale et al., 2019). Initial cell filtering selected cells that expressed >1000 genes. Cells containing high percentages of mitochondrial (> 20%) and

hemoglobin gene (> 0.025%) were also filtered out. Genes included in the analysis were expressed in a minimum of three cells. Only one read per cell was needed for a gene to be counted as expressed per cell. The resulting gene expression matrix was normalized to 10,000 molecules per cell and log transformed (Macosko et al., 2015). Cell-type clusters and marker genes for each cluster were identified using the R v3.6.1 library Seurat v3.1.0 (Butler et al., 2018; Stuart et al., 2019). All clustering was unsupervised without driver genes. The influence of the number of unique molecular identifiers was minimized by regression within the ScaleData function. The following analyses were performed to compare NSCs/progenitors at different stages: *Identification of distinct cell types:* The top 2,000 to 3,000 genes (E12.5, 1730; E18.5, 1935; P14, 2490; and adult, 2842) with highest variability among cells at each stage were used for principal components analysis (see Supplementary Table 1). Cell clusters were determined by the Louvain algorithm. Dimension reduction was performed using the Python implementation of UMAP using the top 18 significant principal components determined by JackStraw plot (Becht et al., 2018). Marker genes were determined for each cluster using the Wilcoxon Rank Sum test within the FindAllMarkers function using genes expressed in a minimum of 10% of cells and fold change threshold of 1.3.

Comparisons of Olig2- and Gsx2-expressing cells in the postnatal SVZ: Feature plots of cells expressing *Olig2* and *Gsx2* were generated using all cells, and the number of single and double expressing cells in each cell cluster was calculated. To examine the relative expression levels of Olig2 and Gsx2 in individual NSCs, cells that belong to aNSC/TAP clusters (cluster 4 for adult and cluster 1 for P14) were isolated, and relative raw integer counts of *Olig2* and *Gsx2* transcripts in each cell were calculated and plotted. Pearson's correlation coefficient was calculated regarding the correlations between the copy numbers of Olig2 and Gsx2 transcripts in each cell among Olig2- and Gsx2-expressing cells.

Comparisons of Olig2-expressing NSCs/progenitors at different stages: Olig2-expressing

NSC/progenitor clusters (E12.5, clusters 0, 2, and 6; E18.5, clusters 1 and 3; P14, clusters 1 and 9; adult, clusters 0 and 4) (see Figure 2 and Supplementary Figure 1) were isolated from each dataset and used for comparison. Their developmental trajectory was visualized with a UMAP plot by combining cells from all stages first and subsequently re-clustering into distinct groups (see Supplementary Tables 2 and 3). The cell cycle kinetics of individual NSCs/progenitors was examined based on the overall expression profile of a set of cell cycle-specific genes at S and G2/M phases (see Supplementary Table 4). Cells were divided into three groups (G0/G1, S, and G2/M phases), and the percentage of cells in each group among total cells was calculated and compared. The activity of signaling and metabolic pathways in NSCs/progenitors at different stages were compared by ReactomeGSA (https://reactome.org; see Griss et al., 2020). First, the average expression level of each gene across Olig2-expressing NSCs/progenitors at each developmental stage was calculated. Subsequently, a gene set variation analysis (GSVA) of these pseudo bulk gene expression levels was performed to calculate scores based on the expression of a set of genes for each molecular pathway for each sample (Hänzelmann et al., 2013). In this calculation, a high positive score is generated when most or all of the genes in a particular pathway are expressed, whereas a low or negative score is generated when few or none of the genes are expressed (Griss et al., 2020). The difference between the minimum and maximum scores per pathway among four developmental stages indicates the extent of the change in the overall activity of the pathway between developmental stages (see Supplementary Table 5). Top 19 pathways that show the largest score differences between different stages and positive scores at the peak stages are plotted on a heatmap in which colors represent the relative pathway scores.

Supplementary References

Battiste, J., Helms, A.W., Kim, E.J., Savage, T.K., Lagace, D.C., Mandyam, C.D., Eisch, A.J., Miyoshi, G., Johnson, J.E. (2007). Ascl1 defines sequentially generated lineage-restricted neuronal and oligodendrocyte precursor cells in the spinal cord. *Development* 134(2): 285-293.

Butler, A., Hoffman, P., Smibert, P., Papalexi, E., Satija, R. (2018). Integrating single-cell transcriptomic data across different conditions, technologies, and species. *Nat Biotechnol* 36(5), 411–420.

DePasquale, E.A.K., Schnell, D.J., Van Camp, P.-J., Valiente-Alandí, Í., Blaxall, B.C., Grimes, H.L., Singh, H., Salomonis, N. (2019). DoubletDecon: Deconvoluting Doublets from Single-Cell RNA-Sequencing Data. *Cell Rep* 29(6), 1718-1727.e8.

Kuwajima, T., Nishimura, I., Yoshikawa, K. (2006). Necdin promotes GABAergic neuron differentiation in cooperation with Dlx homeodomain proteins. *J Neurosci* 26(20): 5383-5392.

Macosko, E.Z., Basu, A., Satija, R., Nemesh, J., Shekhar, K., Goldman, M., Tirosh, I., Bialas, A.R., Kamitaki, N., Martersteck, E.M., et al. (2015). Highly Parallel Genome-wide Expression Profiling of Individual Cells Using Nanoliter Droplets. *Cell* 161(5), 1202–1214.

Nagao, M., Campbell, K., Burns, K., Kuan, C.Y., Trumpp, A., Nakafuku, M. (2008). Coordinated control of self-renewal and differentiation of neural stem cells by Myc and the p19ARF-p53 pathway. *J Cell Biol* 183(7): 1243-1257.

Paxinos, G., Franklin, K.B.J. (2008). *Paxinos and Franklin's the mouse brain in stereotaxic coordinates*. Boston : Elsevier/Academic Press, Amsterdam.

Roychoudhury, K., Salomone J., Qin S., Cain B., Adam M., Potter SS., Nakafuku M., Gebelein B., Campbell K. (2020). Physical interactions between Gsx2 and Ascl1 balance progenitor expansion versus neurogenesis in the mouse lateral ganglionic eminence. *Development* 147(7):dev185348.

Stuart, T., Butler, A., Hoffman, P., Hafemeister, C., Papalexi, E., Mauck, W.M., Hao, Y., Stoeckius, M., Smibert, P., Satija, R. (2019). Comprehensive Integration of Single-Cell Data. *Cell* 177(7), 1888-1902.e21.

Yue T., Xian K., Hurlock E., Xin M., Kernie SG., Parada LF., Lu QR. (2006). A critical role for dorsal progenitors in cortical myelination. *J Neurosci* 26(4):1275-1280.